


# The zircon Hf isotope archive of rapidly changing mantle sources in the south Patagonian retro-arc

**Journal Article****Author(s):**

Ewing, Tanya A.; Müntener, Othmar; [Leuthold, Juerg](#) ; Ramírez de Arellano, Cristóbal; Baumgartner, Lukas P.; Schaltegger, Urs

**Publication date:**

2018

**Permanent link:**

<https://doi.org/10.3929/ethz-b-000305252>

**Rights / license:**

[In Copyright - Non-Commercial Use Permitted](#)

**Originally published in:**

GSA Bulletin, <https://doi.org/10.1130/b31983.1>

# The zircon Hf isotope archive of rapidly changing mantle sources in the south Patagonian retro-arc

Tanya A. Ewing<sup>1,†</sup>, Othmar Müntener<sup>1</sup>, Julien Leuthold<sup>2</sup>, Cristóbal Ramírez de Arellano<sup>3</sup>, Lukas P. Baumgartner<sup>1</sup>, and Urs Schaltegger<sup>4</sup>

<sup>1</sup>*Institute of Earth Sciences, University of Lausanne, 1015 Lausanne, Switzerland*

<sup>2</sup>*Institute of Geochemistry and Petrology, ETH Zürich, 8092 Zurich, Switzerland*

<sup>3</sup>*Faculty of Engineering, Universidad Andres Bello, Santiago, Chile*

<sup>4</sup>*Department of Earth Sciences, University of Geneva, 1205 Geneva, Switzerland*

## ABSTRACT

Rapid changes in geochemical and isotopic signatures of arc-related magmatic products can be used to trace magmatic processes in subduction zones across many scales, from the regional response of magmatism to large-scale geodynamic changes in the subduction system, to the emplacement of single intrusions. In this contribution, we use the south Patagonian subduction system as a natural laboratory to investigate magmatic processes in continental arcs. We use diverse intrusions and dikes from the retro-arc region at 49–51°S to investigate these processes both at the subduction zone scale, and within the exceptionally well-exposed Torres del Paine sheeted intrusion. We present Hf isotope data for zircon from 30 to 12 Ma magmatic units that were emplaced ~50 km inboard of the main subduction-related batholith. These samples record an ~18 m.y. period during which the region experienced profound geodynamic changes, resulting in transient migration of arc magmatism into the retro-arc, which then vanished to be replaced by more alkaline retro-arc magmatism. Integrating published whole rock geochemistry, we show that the Hf isotope signatures of these magmatic units directly record their mantle sources, with negligible assimilation of continental crust into magmas during transport through and storage in the crust. This allows us to trace the appearance and disappearance of the subduction component in the retro-arc mantle. Our data show that migration of calc-alkaline magmatism into the retro-arc produced magmas with a more

enriched Hf isotope composition that was remarkably consistent over ~200 km and >4 m.y. ( $\epsilon_{\text{Hf}(t)}$  of –1 to +2.5). These signatures record addition of subducted continental crust to the mantle wedge during a period of subduction erosion that was associated with arc migration, and show that only a few m.y. of fluxing by a subduction component is sufficient to leave a distinct Hf isotope imprint on a mantle wedge previously unmodified by subduction. The Torres del Paine laccolith was built up by discrete pulses of magmatism in <200 k.y. Our data show isotopic differences between magmatic batches, and an abrupt shift to more juvenile Hf isotope compositions during the buildup of the youngest part of this magmatic complex, recording the rapid input of new mantle-derived melts during its formation. This rapid rejuvenation occurred within  $20 \pm 10$  k.y., demonstrating that different batches of magmatism within a single intrusive complex can tap geochemically distinct mantle reservoirs on very short timescales of <200 k.y.

## 1. INTRODUCTION

Sheeted intrusive complexes offer an opportunity to investigate the architecture of a pluton, and constrain the timing, frequency, and magnitude of successive episodes of magmatism. The traditional view of plutons as large entities emplaced en masse then slowly cooled has been challenged in favor of more complex, polyphase models. Single-crystal U–Pb geochronology of zircon has demonstrated that different units within a single intrusive complex can have resolvable different ages, complementing field evidence for the emplacement of such complexes in discrete magma batches (e.g., Barboni et al., 2015; Broderick et al., 2015; Claiborne et al., 2010; Coleman et al., 2004; Glazner

et al., 2004; Leuthold et al., 2012; Michel et al., 2008; Schaltegger et al., 2009; Schmitt et al., 2011; Schoene et al., 2012). A question that has received less attention is whether different batches of magma within a sheeted complex tap the same reservoir, or are fed by geochemically different sources. Hafnium (Hf) isotopes are a powerful tool to address this question, providing a robust isotopic fingerprint of the magmatic source that traces the relative contributions from continental crust and mantle reservoirs. The mineral zircon is a particularly attractive target for Hf isotope analysis, as it contains weight percent of HfO<sub>2</sub> (Hoskin and Schaltegger, 2003) and is extremely robust both physically and chemically, preserving its Hf isotope signature under all known crustal conditions (Hoskin and Black, 2000; Kinny et al., 1991). Coupled Hf isotope and U–Pb age data can be used to trace changes in magma source composition over time, whether on the scale of a single pluton (e.g., Broderick et al., 2015), a batholith (e.g., Kemp et al., 2007), or the continental crust (e.g., Dhuime et al., 2012).

The Torres del Paine intrusive complex (TPIC) is a shallow crustal sheeted intrusive complex that was emplaced in Patagonia on rapid timescales of ca. 160 k.y. (Leuthold et al., 2012; Michel et al., 2008) (Figs. 1 and 2). Field and geochronological evidence testify to its emplacement in multiple discrete batches of magma (Leuthold et al., 2013; Leuthold et al., 2012; Michael, 1991; Michel et al., 2008). It is spectacularly exposed in three dimensions due to kilometer-scale vertical relief and extensive glacier-denuded outcrops. The TPIC was emplaced in the retro-arc region of a long-lived continental subduction zone in southern Patagonia (South America). In this contribution, we present zircon Hf isotope data for different units from the 12–13 Ma Torres del Paine intrusive complex. We also present Hf

<sup>†</sup>Present address: Institute of Geological Sciences, University of Bern, 3012 Bern, Switzerland; tanya.ewing@geo.unibe.ch

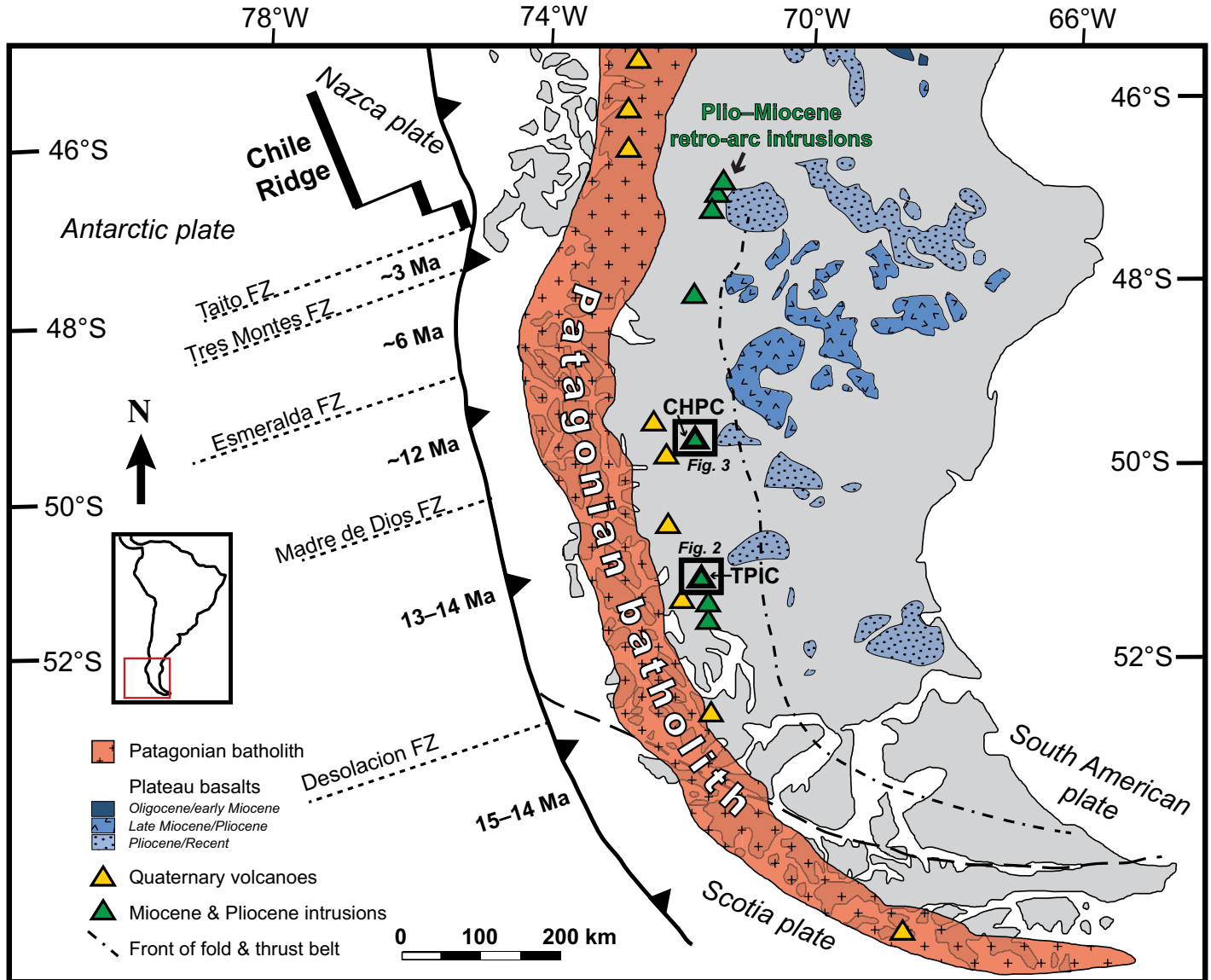


**Figure 1.** Map of southern Patagonia, modified after Ramírez de Arellano et al. (2012), showing the Patagonian batholith, Plio–Miocene intrusions inboard of the batholith, and the Quaternary volcanoes that represent the modern active arc in this area. Plateau basalts after Kay et al. (2004); Eocene plateaus are not shown. The Torres del Paine intrusive complex (TPIC) and Chaltén plutonic complex (CHPC) are shown as triangles with a bold outline. Black rectangles indicate the approximate locations (not to scale) of detailed maps of the two complexes presented in Figures 2 and 3, respectively. The present day positions of the Chile spreading ridge (solid lines), as well as the major fracture zones (FZ) (dashed lines), are shown along with separated segments of the Chile ridge subducted at different times, are shown along with the time of subduction for each segment (after Cande and Leslie, 1986; Guivel et al., 2006; Kay et al., 2004).

isotope data for a number of small intrusions and dikes that are found within ~15 km of the TPIC, with ages spanning 12–30 Ma; and for a 16–17 Ma intrusive complex (Chaltén plutonic complex) that crops out ~200 km to the north. Our data resolve the evolving Hf isotope signature of retro-arc magmatism over a ca. 18 m.y. period of its history, during which the region witnessed profound geodynamic changes associated with changing convergence rates and subduction of an active spreading ridge; and

on short timescales (<200 k.y.) during the progressive emplacement of a single sheeted intrusive complex within the retro-arc. We demonstrate that the longer-term evolution of the Hf isotope composition of magmatism on a regional scale is unaffected by crustal assimilation, with remarkably consistent  $\epsilon_{\text{Hf}(t)}$  on large temporal and spatial scales of ca. 4 m.y. and 200 km. Our data thus allow us to trace changing crustal inputs into the retro-arc mantle of a single continental arc over a ca. 18 m.y. period,

and show that more crustal Hf isotope compositions record addition of a subducted continental crustal component to the mantle wedge. Our data reveal an abrupt shift to more juvenile Hf isotope compositions in the youngest part of the TPIC, recording input of more primitive melts derived directly from the mantle. We thus demonstrate that different batches of magma within a single intrusive complex can tap distinct mantle geochemical reservoirs, even on 10 k.y. timescales.

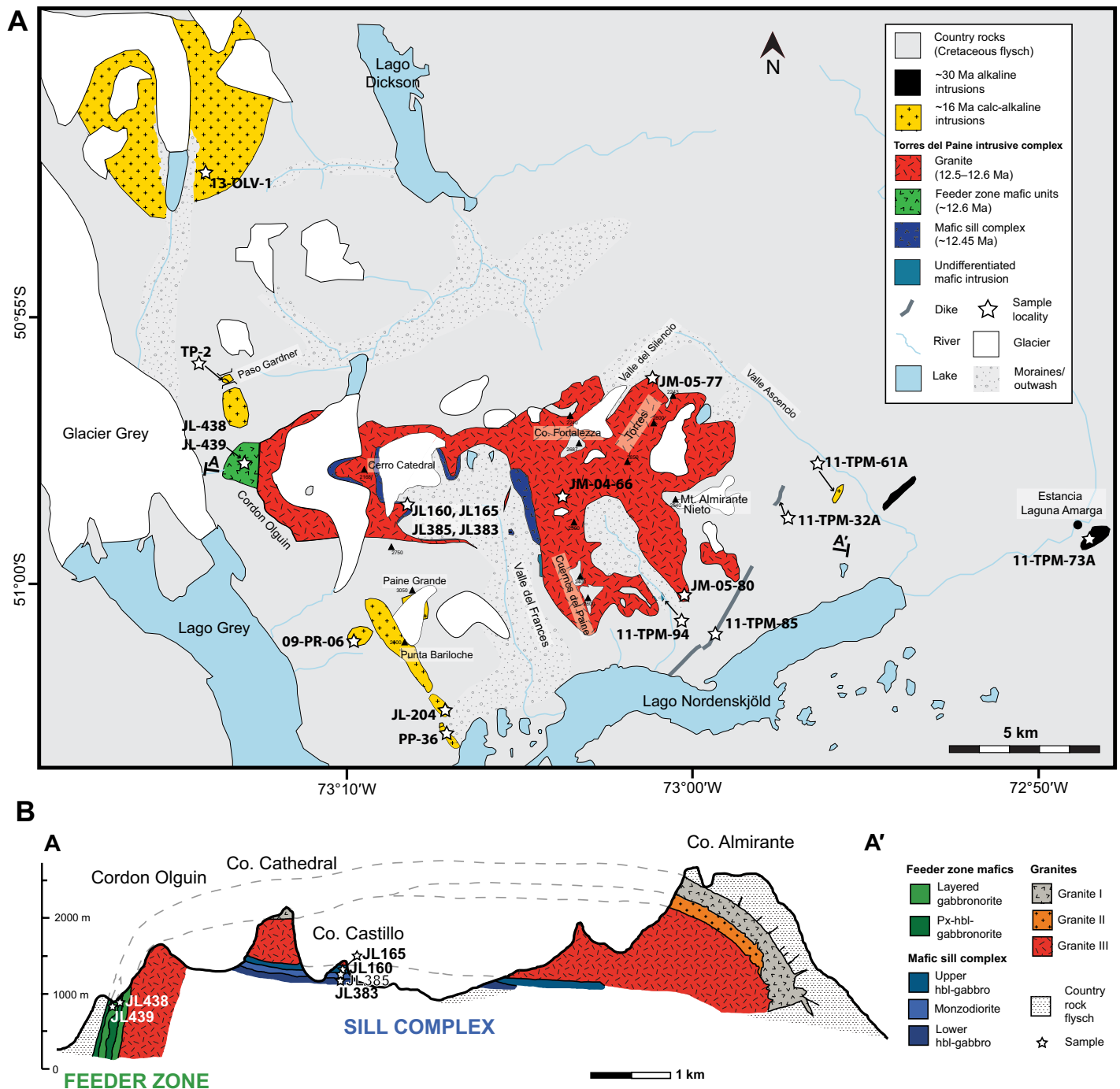


**Figure 2.** (A) Geological map of the Torres del Paine area, southern Patagonia, Chile, showing location of samples analyzed in this study. The map is based on an aerial photograph, rather than a topographic map; latitudes and longitudes are approximate. A–A' indicates the location of the cross section illustrated in Figure 2B. (B) Cross section through the Torres del Paine intrusive complex after Leuthold et al. (2012) and Michel et al. (2008).

## 2. GEOLOGICAL SETTING

Along the western margin of Patagonia (South America), subduction has been ongoing since the Late Jurassic in a complex and evolving geodynamic setting (e.g., Breitsprecher and

Thorkelson, 2009; Cande and Leslie, 1986; Hervé et al., 2007). Highly oblique convergence from at least 42 Ma changed abruptly to much faster, nearly orthogonal convergence at ca. 26 Ma after the breakoff of the Farallon plate (Cande and Leslie, 1986; Somoza, 1998).

Convergence slowed again at ca. 16 Ma but remained largely orthogonal (Breitsprecher and Thorkelson, 2009; Somoza, 1998). Beginning at ca. 15 Ma, the active spreading ridge between the Nazca and Antarctic plates (Chile ridge) arrived at the convergent margin in southern-

most Patagonia (~53°S) and began to subduct (Breitsprecher and Thorkelson, 2009; Cande and Leslie, 1986). The associated triple junction migrated northwards in episodic large jumps to reach its present position at ~47°S, and ridge subduction occurred at the latitude of Torres del Paine at ca. 13–14 Ma (Cande and Leslie, 1986; Guivel et al., 2006; Fig. 1).

South of the present-day triple junction (~47°S), arc magmatism associated with this long-lived subduction is represented by (1) the voluminous calc-alkaline South Patagonian batholith, which was built up episodically from ca. 160 Ma, with the last period of abundant magmatism from 25 Ma to 16 Ma (Hervé et al., 2007) and (2) the Holocene volcanoes of the Austral Volcanic Zone, which represent the modern volcanic arc and are located ~50 km inboard of the South Patagonian batholith (Ramírez de Arellano et al., 2012; Stern and Kilian, 1996) (Fig. 1). To the east, voluminous basaltic plateaus with alkaline to transitional alkaline chemistry are widespread throughout the retro-arc region in southern Patagonia both north and south of the present-day triple junction (e.g., Espinoza et al., 2005; Forsythe and Prior, 1992; Gorring et al., 1997; Guivel et al.,

2006; Kay et al., 2004; Ramos and Folguera, 2011; Ramos and Kay, 1992) (Fig. 1). We use the term “retro-arc,” rather than back-arc, to indicate the area immediately inboard of the main arc batholith, since in South America this area is represented by unrifted continental crust. South of the present-day triple junction, a roughly linear series of intrusions crops out episodically over ~800 km in the retro-arc region, ~50–100 km inboard of the batholith, but trench-wards of the basaltic plateaus (e.g., Leuthold et al., 2013; Michael, 1991; Ramírez de Arellano et al., 2012) (Fig. 1). These intrusions range in ages from ca. 3 Ma to 30 Ma, with no systematic variation in age from south to north (Ramírez de Arellano et al., 2012, and references therein). They have heterogeneous geochemical compositions ranging from calc-alkaline to transitional alkaline (Espinoza et al., 2010; Leuthold et al., 2013; Ramírez de Arellano et al., 2012). We refer to this series of small intrusions as “retro-arc intrusions,” noting the fact that they are diverse both in age and chemistry precludes a direct link between all of them in terms of either genesis or process. We studied two of these retro-arc intrusions, described in detail below.

**2.1. Studied Retro-Arc Intrusions**

The Chaltén plutonic complex is an ultra-mafic to granitic intrusive complex which crops out over ~62 km<sup>2</sup> around Cerro Fitz Roy at ~49°S (Ramírez de Arellano et al., 2012) (Figs. 1 and 3). The country rock into which it was emplaced comprises metasedimentary rocks of the Paleozoic Eastern Andes Metamorphic Complex, and a range of strongly deformed sedimentary, volcanosedimentary, and volcanic units ranging in age from Jurassic to Cretaceous (Augustsson et al., 2006; Ramírez de Arellano et al., 2012; see Section DR1 for descriptions of individual formations). On the basis of detailed fieldwork and high-precision thermal ionization mass spectrometry (TIMS) U–Pb geochronology of zircon, Ramírez de Arellano et al. (2012) distinguished eight major intrusive units (Fig. 3) with ages ranging from 16.90 ± 0.05 Ma to 16.37 ± 0.02 Ma, described in more detail in Section DR1. All of these units have calc-alkaline major and trace element geochemistry typical of subduction-related magmatism, indistinguishable from the Patagonian batholith (Ramírez de Arellano et al., 2012). The Chaltén plutonic complex

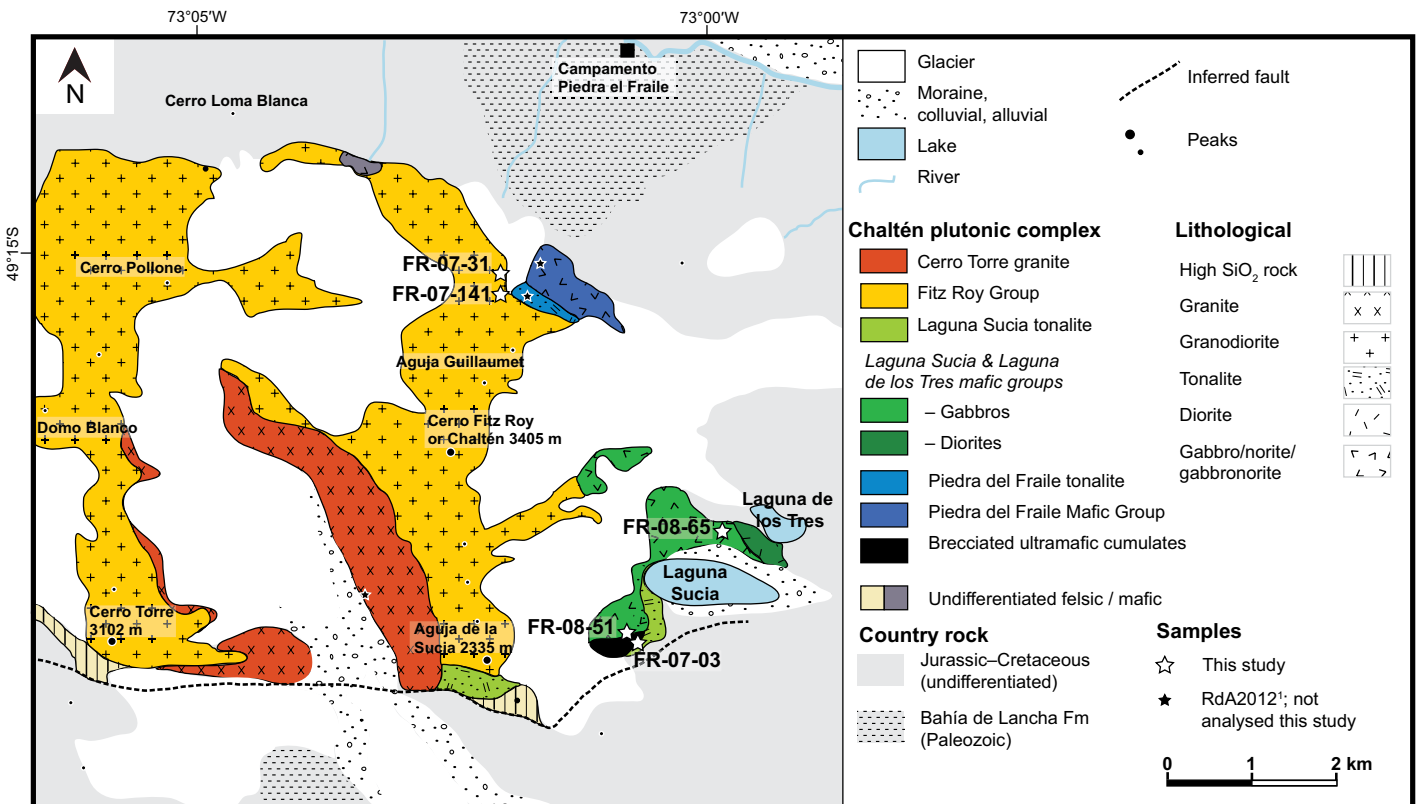


**Figure 3.** Geological map of the Chaltén plutonic complex, southern Patagonia, Argentina, after <sup>1</sup>Ramírez de Arellano et al. (2012). In the legend, units within the Chaltén plutonic complex are arranged from youngest (Cerro Torre granite) to oldest (ultramafic cumulates), as described by Ramírez de Arellano et al. (2012).

is interpreted as a typical arc pluton, and its position ~100 km inboard of the main South Patagonian batholith has been explained by the progressive continent-wards migration of arc magmatism from ca. 20 Ma to 17 Ma as a result of shortening and subduction erosion associated with rapid convergence (Ramírez de Arellano et al., 2012).

The Torres del Paine intrusive complex (TPIC) crops out some 200 km south of the Chaltén plutonic complex, at ~51°S (Fig. 1). The TPIC is a shallow crustal bimodal intrusion in which a significant volume (~88 km<sup>3</sup>) of mafic and granitic magma was emplaced on short timescales of 162 ± 11 k.y. (Leuthold et al., 2012; Michel et al., 2008). It was emplaced into the Late Cretaceous–Tertiary sedimentary Cerro Toro and Punta Barossa formations, both of which are turbiditic sequences made up of alternating sandstone and pelite, with subordinate carbonates (Leuthold et al., 2013; Michael, 1991; Wilson, 1991). The middle and lower crust in this region is inferred to be made up of Paleozoic metamorphic basement (Fosdick et al., 2011), presumably dominantly of the metasedimentary Eastern Andes Metamorphic Complex (Augustsson et al., 2006; Hervé et al., 2003). Detailed study of field relations has shown that the TPIC was built up in a series of discrete magma batches, producing the observed sheeted geometry (Leuthold et al., 2012).

The TPIC can be divided into two parts, with distinct ages resolved by high-precision single-grain U–Pb dating of zircon. The sub-horizontally layered *sill complex* comprises three voluminous granitic units underplated by a *mafic sill complex* dominated by hornblende gabbros and (monzo)-diorites (Leuthold et al., 2012; Michel et al., 2008) (Fig. 2). The granite units have ages ranging from 12.49 ± 0.01 Ma to 12.58 ± 0.01 Ma (Michel et al., 2008; recalculated by Leuthold et al., 2012), whereas four units from the mafic sill complex gave ages ranging from 12.472 ± 0.009 to 12.431 ± 0.006 Ma (Leuthold et al., 2012) (Fig. 2). The vertically layered *feeder zone* crops out in the westernmost TPIC, and comprises mafic units (dominantly gabbro-norites) and Granite III, which is the only unit to crop out in both the sill complex and the feeder zone (Fig. 2). Mafic units from the feeder zone are resolvably older than the mafic sill complex, and have ages of 12.593 ± 0.009 Ma to 12.587 ± 0.009 Ma (Leuthold et al., 2012).

All units from the TPIC have “transitional alkaline” whole rock chemistry (Leuthold et al., 2013) that is intermediate between the calc-alkaline batholith to the west (Hervé et al., 2007) and the truly alkaline plateau basalts to the east

that have chemistry similar to ocean island basalts (OIBs) (Espinoza et al., 2005; Guivel et al., 2006). TPIC samples plot broadly around the boundary between alkaline and sub-alkaline on a TAS diagram, but are also distinct from calc-alkaline samples in trace element ratios used to fingerprint subduction components (e.g., La/Nb; Leuthold et al., 2013). The distinct transitional alkaline chemistry of the TPIC demonstrates that, in contrast to the Chaltén plutonic complex, it is not the product of typical subduction-related magmatism.

## 2.2. Other Intrusions and Dikes in the Torres Del Paine Region

A number of smaller intrusions that are not directly related to the TPIC are found within 1–15 km of the complex (Fig. 2). The majority of these are gabbroic to granitic intrusions that have calc-alkaline chemistry more similar to the South Patagonian batholith and the Chaltén plutonic complex than to the TPIC (Müntener et al., 2018). They have tightly clustered U–Pb ages from 15.7 ± 0.4 Ma to 16.5 ± 0.2 Ma (Müntener et al., 2018). Analogous to the Chaltén plutonic complex, these intrusions are interpreted as the product of migration of arc-related magmatism some 50 km inboard of the main batholith. A small ca. 30 Ma alkaline gabbro crops out ~15 km east of the TPIC, and has distinct, alkaline chemistry with trace element patterns similar to those of typical OIBs (Müntener et al., 2018). Several generations of dikes are also found in the region. Four generations of dikes were distinguished on the basis of geochemistry, geochronology, and field relations, the oldest three of which have been related genetically to the ca. 30 Ma alkaline intrusions, ca. 16 Ma calc-alkaline intrusions, and ca. 12.5 Ma TPIC, respectively (Müntener et al., 2018). The fourth generation comprises recent alkaline dikes that are mantle xenolith-bearing (Müntener et al., 2018). In this study, only dikes from the ca. 12.5 Ma generation were analyzed, as well as one small monzonite intrusion with a ca. 12 Ma age (Fig. 2; Müntener et al., 2018).

## 3. SAMPLES

We analyzed twenty-four samples that were previously collected, described in detail, and dated by Leuthold et al. (2012), Michel et al. (2008), Müntener et al. (2018), and Ramírez de Arellano et al. (2012). Nine samples from the Torres del Paine intrusive complex sampled the mafic sill complex, mafic units from the feeder zone, and two of the TPIC granite units (I and III) (Fig. 2). Ten samples collected from

the area immediately surrounding the TPIC (≤15 km distant) sampled small intrusions and dikes distinct from the TPIC: the ca. 30 Ma alkaline Amarga gabbro, six 17–16 Ma calc-alkaline intrusions, a small exposure of a ca. 12 Ma monzonite intrusion, and two bimodal dikes that cut metasedimentary rocks of the Cerro Toro Formation (Fig. 2). Five samples from the Chaltén plutonic complex sampled five different units ranging from gabbro-noritic to granitic in composition. Lithological data and previously published geochronology for the analyzed samples are summarized in Table 1, and samples are described in more detail in Section DR1.

## 4. METHODS

### 4.1. Solution MC-ICPMS Instrumental

Hf isotope composition was determined by solution multicollector inductively coupled plasma mass spectrometer (MC-ICPMS) on the Neptune Plus at the University of Geneva (UNIGE), Switzerland, with sample introduction by an Aridus desolvating nebuliser. Hf isotope analysis was performed on solutions obtained from single zircon grains dated by Leuthold et al. (2012) and Ramírez de Arellano et al. (2012) using isotope dilution thermal ionization mass spectrometry (ID-TIMS) U–Pb techniques. The analyzed solutions represent the trace element fractions of the TIMS U–Pb anion exchange column chemistry that have been dried down and stored over four years. No further ion chromatographic separation has been applied to these element fractions, which were made up to a suitable volume for analysis using 2% HNO<sub>3</sub> with a trace of HF. Nine masses were measured: <sup>172</sup>Yb, <sup>173</sup>Yb, <sup>175</sup>Lu, <sup>176</sup>(Hf+Yb+Lu), <sup>177</sup>Hf, <sup>178</sup>Hf, <sup>179</sup>Hf, <sup>180</sup>(Hf+Ta+W), and <sup>181</sup>Ta.

Analytical blanks were monitored by analysis of aliquots of the 2% HNO<sub>3</sub> + trace HF, generally after every 4–7 sample solutions. Blanks were found to vary significantly and nonlinearly, making it difficult to accurately constrain the true analytical blank for most analyses. Analytical blanks were therefore not subtracted except for two low-Hf analyses that had a blank measurement immediately prior. For these two analyses, blanks accounted for ~0.07% and 0.12%, respectively, of the signal on each Hf isotope. For all other solutions, high signal to blank ratios meant that subtracting a blank would make a negligible difference (≤0.2 E<sub>Hf</sub>-units). The range of measured blanks across all solution sessions was 0.001–0.009 V on <sup>178</sup>Hf, whereas for sample analyses intensities of 1–29 V were measured on the same isotope.

TABLE 1. LITHOLOGICAL AND PUBLISHED GEOCHRONOLOGICAL INFORMATION FOR THE ANALYSED SAMPLES FROM PATAGONIA, SOUTH AMERICA

Sample	Unit	Lithology	Sampling area	Age (Ma)	Hf
<b>Torres del Paine intrusive complex</b>					
JL438	Feeder zone	Pegmatite segregation in layered gabbro	Cordon Olguin	12.587 ± 0.009 <sup>1</sup>	S
JL439	Feeder zone	Pegmatite segregation in Px-Hbl gabbro	Cordon Olguin	12.593 ± 0.009 <sup>1</sup>	S
JL383	Mafic sill complex	Lower hornblende gabbro	Valle del Frances	12.472 ± 0.009 <sup>1</sup>	S
JL385	Mafic sill complex	Diorite sill	Valle del Frances	12.453 ± 0.010 <sup>1</sup>	S
JL160	Mafic sill complex	Upper hornblende gabbro	Valle del Frances	12.434 ± 0.009 <sup>1</sup>	S
JL165	Mafic sill complex	Layered diorite	Valle del Frances	12.431 ± 0.006 <sup>1</sup>	S
JM-05-77	Granite laccolith	Granite I	Valle Ascencio	12.58 ± 0.02 <sup>1,2</sup>	LA
JM-05-80	Granite laccolith	Granite I	Valle Bader	12.58 ± 0.01 <sup>1,2</sup>	LA
JM-04-66	Granite laccolith	Granite III	Valle del Frances	12.49 ± 0.02 <sup>1,2</sup>	LA
<b>Other intrusions and dikes—Torres del Paine region</b>					
11-TPM-94	ca. 12 Ma monzonite (small exposure)	Monzonite	Valle Bader	12.4 ± 0.2 <sup>3</sup>	LA
11-TPM-32A	Bimodal dikes	Microgranite + basaltic andesite	SW flank Mt. Almirante	12.8 ± 0.2 <sup>3</sup>	LA
11-TPM-85	Bimodal dikes	Microgranite	SW flank Mt. Almirante	12.3 ± 0.2 <sup>3</sup>	LA
13-OLV-1	Calc-alkaline intrusions (Olvidado complex)	Monzogranite	Valle Olvidado	15.7 ± 0.4 <sup>3</sup>	LA
13-TP2-1	Calc-alkaline intrusions	Granodiorite	Paso John Gardner	15.9 ± 0.4 <sup>3</sup>	LA
PP-36	Calc-alkaline intrusions	Granitic pegmatite, intermingled diorite	SSE flank Punta Bariloche	16.4 ± 0.2 <sup>3</sup>	LA
07-JL-204	Calc-alkaline intrusions	Gabbro	SSE flank Punta Bariloche	16.5 ± 0.2 <sup>3</sup>	LA
09-PR-06	Calc-alkaline intrusions	Granite	W ridge Cumbre Central	16.1 ± 0.2 <sup>3</sup>	LA
11-TPM-61A	Calc-alkaline intrusions	Diorite	Valle Ascencio	16.2 ± 0.2 <sup>3</sup>	LA
11-TPM-73A	Amarga alkaline gabbro	Monzogabbro	Laguna Amarga	ca. 29–30 Ma <sup>3</sup>	LA
<b>Chaltén plutonic complex</b>					
FR-08-65	Laguna de los Tres mafic group	Gabbro	Laguna de los Tres	16.83 ± 0.04 <sup>4</sup>	S
FR-08-51	Laguna Sucia mafic group	Gabbro	Laguna Sucia	16.78 ± 0.10 <sup>4</sup>	S
FR-07-03	Laguna Sucia group	Tonalite	Laguna Sucia	16.70 ± 0.06 <sup>4</sup>	S
FR-07-31	Fitz Roy group	Granodiorite	Piedra del Fraile	16.58 ± 0.02 <sup>4</sup>	S
FR-08-141	Fitz Roy group	Banded granite	Piedra del Fraile	16.58 ± 0.03 <sup>4</sup>	S

Notes: Ages from <sup>1</sup>Leuthold et al. (2012), <sup>2</sup>Michel et al. (2008), <sup>3</sup>Müntener et al. (2018), and <sup>4</sup>Ramírez de Arellano et al. (2012). For detailed sample descriptions the reader is also directed to these references. More detailed descriptions of sampling locations for the other intrusions and dikes in the Torres del Paine region are given in Section DR1. "Hf" indicates the method used to determine Hf isotope composition: Solution (S) or laser ablation (LA) multicollector inductively coupled plasma mass spectrometry.

Analyses were normalized to the average value measured in each session for JMC-475 40 ppb Hf solution standard (analyzed every 4–7 analyses), relative to the reference value of 0.282160 (Nowell et al., 1998). This correction was always  $\leq 0.35 \epsilon_{\text{Hf}}$ -units (Fig. DR1<sup>1</sup>). The internal precision of most analyses was significantly better than the external reproducibility of JMC-475 solution measurements in the same session. The errors on analyses were therefore forced to equal the reproducibility of JMC-475 analyses in the same session at the two standard deviation (2 S.D.) level, except for analyses that had internal errors larger than this. For calculation of weighted means,  $2\sigma$  errors on each analysis were forced to  $0.7 \epsilon_{\text{Hf}}$ -units, which is the 2 S.D. external reproducibility of nine analyses of JMC-475 doped with Yb measured in one session. The external reproducibility of this Yb-doped JMC-475 is significantly worse than that of Yb-free JMC-475 ( $0.3 \epsilon_{\text{Hf}}$ -units 2 S.D.; Fig. DR1) but is a more realistic estimate of the reproducibility that can be expected for our Yb-bearing zircon solutions.

<sup>1</sup>GSA Data Repository item 2018281, Sections DR1–DR3 (additional descriptions of samples, methodology, and the potential sources of the crustal component identified in magmatic rocks analysed in this study); Figures DR1–DR13; and Tables DR1–DR4, is available at <http://www.geosociety.org/datarepository/2018> or by request to [editing@geosociety.org](mailto:editing@geosociety.org).

## 4.2. Laser Ablation MC-ICPMS Instrumental

In situ Hf isotope measurements were performed on epoxy mounts prepared by Müntener et al. (2018), except for samples JL-204 and three samples previously dated by TIMS (JM-04-66, JM-05-77, and JM-05-80), for which new zircons were handpicked from existing mineral separates (Michel et al., 2008; Müntener et al., 2018). These zircons were mounted in epoxy, polished to expose their mid-sections, and imaged in transmitted light on a petrographic microscope and in cathodoluminescence (CL) on a CamScan MV2300 scanning electron microscope at the University of Lausanne, Switzerland, with 10 kV accelerating voltage, probe current of  $\sim 0.7$  nA, and a working distance of  $\sim 45$  mm. All Hf isotope analyses were guided by CL images (Fig. 4); wherever these suggested more than one generation of zircon growth all possible types of zones were targeted.

In situ Hf isotope analysis by laser ablation MC-ICPMS employed the same Neptune Plus at UNIGE, but coupled to a Photon Machines "Analyte G2" 193 nm laser ablation system connected to a HelEx II two-volume cell. Helium is introduced directly into the cell, with addition of a small flow of nitrogen to the sample gas upstream of the cell (Durrant, 1994; Eggins et al., 1998). Nine masses were measured in

static mode: <sup>171</sup>Yb, <sup>173</sup>Yb, (<sup>174</sup>Yb+<sup>174</sup>Hf), <sup>175</sup>Lu, (<sup>176</sup>Hf+<sup>176</sup>Yb+<sup>176</sup>Lu), <sup>177</sup>Hf, <sup>178</sup>Hf, <sup>179</sup>Hf, and <sup>181</sup>Ta. Analyses were conducted with a circular laser spot of 30 or 50  $\mu\text{m}$  diameter, a repetition rate of 5 Hz, and 100% energy (corresponding to 6.05 J/cm<sup>2</sup>). Analytical blanks were measured after every  $\sim 10$  analyses by collecting data without ablating. No systematic drift in blank values was observed in any session. Average intensities from the nearest blank measurement were subtracted from measured intensities for each isotope in sample analyses. Measured blanks ranged from  $-0.00003$  V to  $0.00006$  V on <sup>178</sup>Hf across all laser ablation sessions. Signals on <sup>178</sup>Hf during sample analyses ranged from 1 to 9 V. Further details of analytical protocol generally followed Ewing et al. (2011) and are described in online appendix Section DR2 (see footnote 1).

The instrument was tuned for sensitivity and peak shape on NIST-610 synthetic glass. The Mudtank natural zircon standard (low Yb) and the MUN-4 high-Yb synthetic zircon of Fisher et al. (2011) were used to tune the instrument for accuracy across a wide range of rare earth element (REE) concentrations, ensuring that the two standards were close to their nominal values, and offset from them by a similar amount. The gas flows in the cell (two He flows and N<sub>2</sub>) proved particularly critical in this respect. A series of natural and synthetic zircons with a wide range of Yb/Hf were analyzed reg-

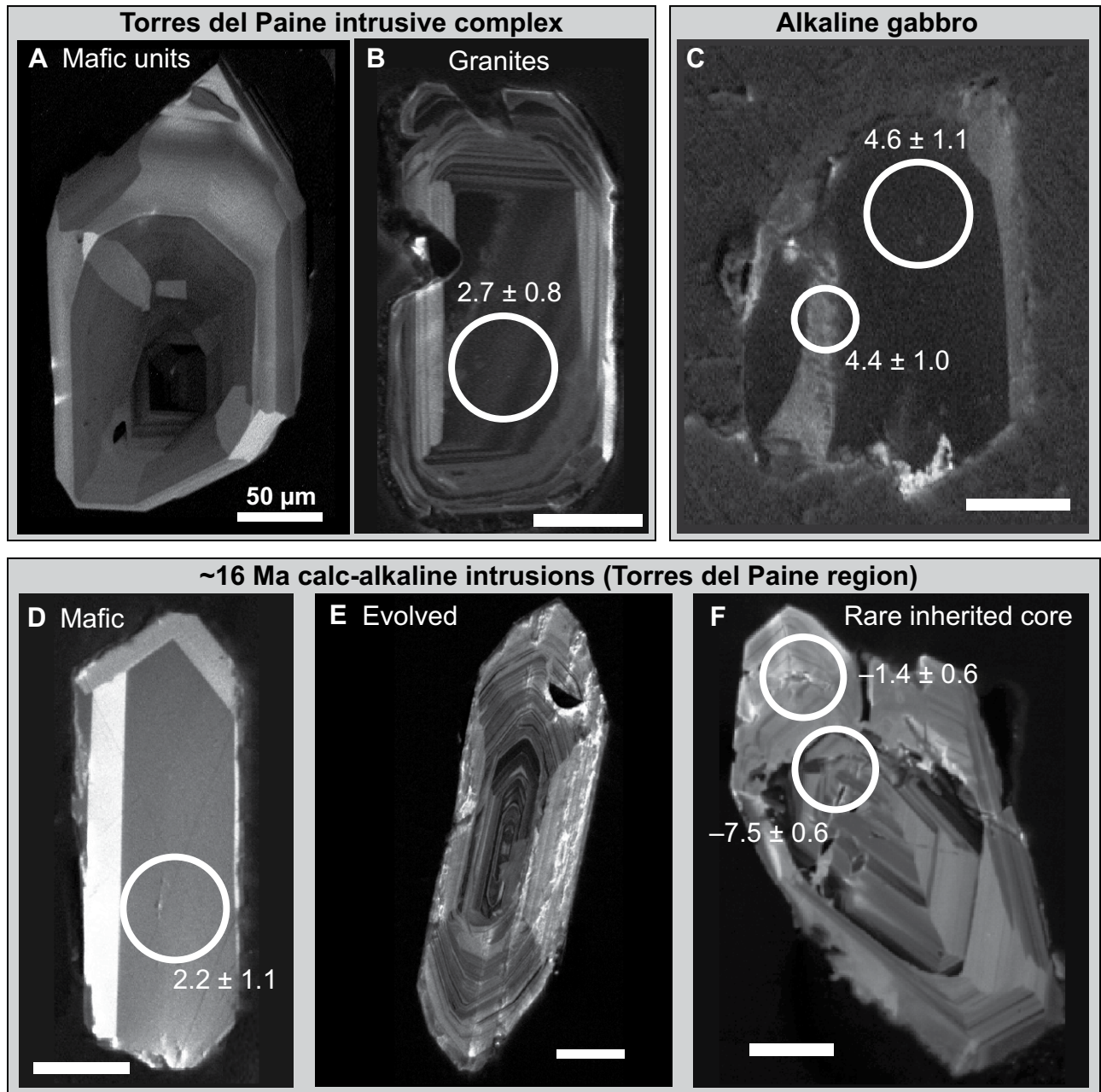


**Figure 4.** Representative cathodoluminescence images of zircon for the main groups of magmatic rocks studied in southern Patagonia. Zircons from evolved lithologies typically show oscillatory zoning, whereas zircons from more mafic lithologies are characterized by paneled or sector zoning. Scale bar is 50  $\mu\text{m}$  in all images. White circles show LA-MC-ICPMS spots, with the measured  $\epsilon_{\text{Hf}(t)}$  indicated. Although no mafic Torres del Paine intrusive complex units were analyzed in situ, a representative zircon from these units is shown for comparison. The pictured zircons are from samples (A) JL385, (B) JM-05-77, (C) TPM-73, (D) 11-TPM-61A, (E) 13-TP2-1, and (F) 09-PR-06.

ularly throughout each session. Natural zircon standards Mudtank, Plešovice, Temora-2, and in some sessions GJ-1 were used as primary standards. Sample analyses were normalized to the average offset of all natural standards from their nominal values (Morel et al., 2008; Sláma et al., 2008; Woodhead and Hergt, 2005). This correction was always  $\leq 1.5 \epsilon_{\text{Hf}}$ -units, with re-

producibility (2 S.D.) of all standards of 1.1  $\epsilon_{\text{Hf}}$ -units or better in all sessions (Table DR3; see footnote 1). The relative error (2 S.D.) of all natural standard analyses was propagated in quadrature onto the analytical errors of each unknown analysis. Synthetic zircons doped with REE were monitored as secondary standards (see below).

#### 4.3. Mass Bias Correction (Solution and Laser Ablation)

For both solution and laser ablation analyses, mass bias was corrected using an exponential law (Russell et al., 1978). Mass bias coefficients were measured for both Hf (relative to  $^{179}\text{Hf}/^{177}\text{Hf}$  of 0.7325; Patchett and Tatsumoto, 1981) and Yb



(following Woodhead et al., 2004). The Yb mass bias coefficient  $\beta_{Yb}$ , calculated from  $^{173}Yb/^{172}Yb$  for solution and  $^{173}Yb/^{171}Yb$  for laser ablation, was also used to correct mass bias for Lu, which has only one interference-free isotope. An external Yb mass bias correction (after Ewing et al., 2011) was used for low-Yb zircons in solution and some laser ablation sessions (Yb-free JMC-475, MUN-0, Mudtank, and some low-Yb sample solutions; Tables DR1, DR3 and DR4; see footnote 1). For synthetic zircon with very high and zoned Yb contents (MUN-4) in two sessions,  $\beta_{Yb}$  was calculated for each cycle of data acquisition (~1 s) rather than calculating a  $\beta_{Yb}$  from the average  $^{173}Yb/^{171}Yb$  across the whole analysis (following Fisher et al., 2014; Woodhead et al., 2004), as this significantly improved  $^{176}Hf/^{177}Hf$  precision. In all other cases an average  $\beta_{Yb}$  (after Iizuka and Hirata, 2005) gave superior precision and was employed.  $^{178}Hf/^{177}Hf$ , which has no isobaric interferences, was monitored to check the effectiveness of the mass bias correction. No relationship is observed between the ratio of interest ( $^{176}Hf/^{177}Hf$ ) and  $^{178}Hf/^{177}Hf$  for either solution or laser ablation analyses (Figs. DR5 and DR7; see footnote 1), confirming the accuracy of the mass bias correction.

#### 4.4. Isobaric Interference Correction and Choice of Yb Isotope Ratios

The correction for isobaric interference from Yb is the biggest challenge for accurate measurement of Hf isotope ratios (e.g., Fisher et al., 2014). As such, the choice of stable Yb isotope ratios used to strip this interference is critical. A range of values exists for these ratios in the literature (e.g., Amelin and Davis, 2005; Chu et al., 2002; Segal et al., 2003; Thirlwall and Anczkiewicz, 2004), with no consensus on which are the most appropriate. It was recently argued that the true values of stable Yb isotope ratios may be less important than finding the appropriate values to give accurate interference corrections for a given instrument and/or technique (Fisher et al., 2011; Kemp et al., 2009).

We tested the effect of different Yb ratios on solution and laser ablation data (Fig. 5). In agreement with Fisher et al. (2011), we find that our MC-ICPMS required the use of different Yb isotope ratios for solution and laser ablation modes to obtain accurate interference-corrected  $^{176}Hf/^{177}Hf$ . We corrected analyses for isobaric interferences on  $^{176}Hf$  using the Yb

and Lu ratios of Thirlwall and Anczkiewicz (2004; TIMS Yb values) for solution mode, and of Chu et al. (2002) for laser ablation. Using these ratios, standards with a wide range of Yb/Hf gave  $^{176}Hf/^{177}Hf$  within error of their nominal values, and there is no relationship between  $^{176}Hf/^{177}Hf$  and Yb/Hf for analyses of any samples or standards across the large range of Yb/Hf they cover (Fig. 5; Figs. DR2, DR3, DR4, and DR6; see footnote 1), demonstrating that isobaric interferences from Yb and Lu have been accurately corrected (e.g., Fisher et al., 2014). In contrast, use of the Thirlwall and Anczkiewicz (2004) Yb ratios for laser ablation or the Chu et al. (2002) ratios for solution produced a dramatic systematic correlation of  $^{176}Hf/^{177}Hf$  with Yb/Hf, with measured values differing by up to 9  $\epsilon_{Hf}$ -units from the nominal value (Figs. 5A, 5B). These data decisively demonstrate that the same Yb ratios cannot be used for the two sampling modes on our instrument.

The accuracy of the Yb interference correction was confirmed by analysis of three aliquots of JMC-475 40 ppb Hf solution doped with varying volumes of 50 ppb Yb solution analyzed in triplicate in one solution session; and regular analysis of synthetic zircons doped with varying degrees of REE including Yb and Lu (supplied by Fisher et al., 2011) as secondary standards in all laser ablation sessions. The Yb-doped JMC-475 had  $^{173}Yb/^{177}Hf$  of 0.13–0.15 (cf 0.04–0.20 for zircons from the samples), and showed no systematic difference in  $^{176}Hf/^{177}Hf$  from Yb-free JMC-475. Previously, accurate solution Hf isotope measurements on our instrument were reported for natural zircon standards Temora and Plešovice processed only through U–Pb column chemistry (D’Abzac et al., 2016). The accuracy of these results for zircon standards confirms that reliable measurement of the Hf isotope composition of zircon is possible without complete matrix removal (D’Abzac et al., 2016). The synthetic zircons analyzed by LA-MC-ICPMS included MUNZirc 4 (Fisher et al., 2011; here referred to as “MUN-4”), which has much higher REE contents than almost all sample zircons analyzed. Any analyses of sample zircons with Yb/Hf higher than MUN-4 were discarded, as were analyses of sample zircons with Yb/Hf comparable to MUN-4 in one two-day session in which this standard only gave inaccurate values. Excluding MUN-4 analyses from this session, the average  $^{176}Hf/^{177}Hf$  in each session for analyses of synthetic zircons across all REE contents was within error of the nominal value of 0.282135 (Fisher et al., 2011; Table DR4; see footnote 1).

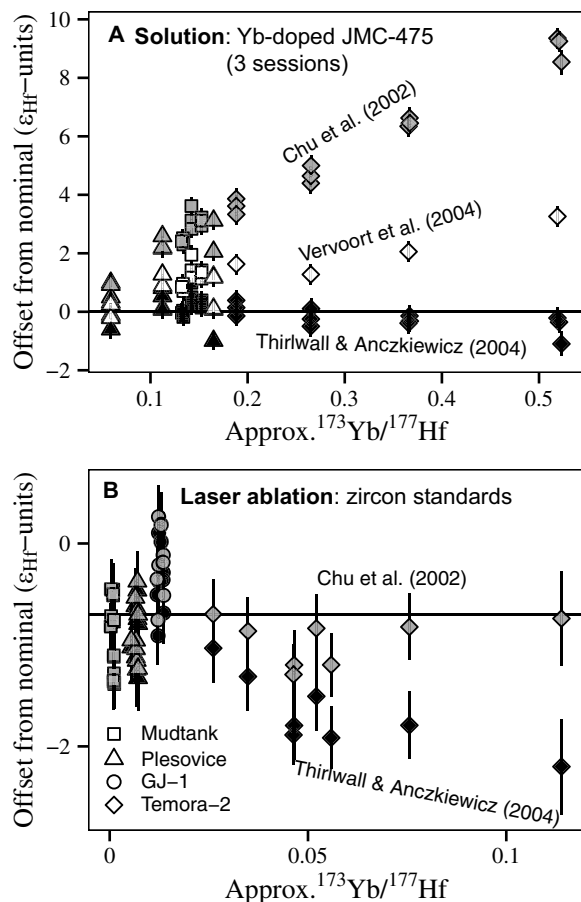


**Figure 5.** Effect of the choice of stable Yb isotope ratios on the accuracy of  $^{176}Hf/^{177}Hf$  of standards. For clarity, not all Yb ratios tested were plotted here. Symbol color indicates the published Yb isotope ratios used to process data: Thirlwall and Anczkiewicz (2004; black), Chu et al. (2002; gray), and Vervoort et al. (2004; white). (A) JMC-475 solution doped with variable amounts of Yb and analyzed in three sessions, normalized to undoped JMC-475. Squares are session 3 of this study (Table DR1; see footnote 1); diamonds and triangles are two sessions not presented here. (B) Primary zircon standards analyzed in a single preliminary LA-MC-ICPMS session (data available on request). Laser data have not been normalized to a standard; black line indicates the average offset of standards used to normalize unknowns in this session.

#### 4.5. Calculation of Initial $\epsilon_{\text{Hf}}$

Initial  $\epsilon_{\text{Hf}}$  ( $\epsilon_{\text{Hf}(t)}$ ) was calculated using the chondritic uniform reservoir (CHUR) parameters of Bouvier et al. (2008) and the  $\lambda_{\text{Lu}}$  of Söderlund et al. (2004). For solution analyses,  $\epsilon_{\text{Hf}(t)}$  was calculated using the TIMS U–Pb age for the same single-zircon solution, taken from Leuthold et al. (2012) or Ramírez de Arellano et al. (2012). Sample  $\epsilon_{\text{Hf}(t)}$  was calculated by taking the weighted mean of  $\epsilon_{\text{Hf}(t)}$  calculated in this way for single zircons. For LA-MC-ICPMS analyses, not all analyses were on a domain previously dated by U–Pb, and the sample age (Müntener et al., 2018; Michel et al., 2008, recalculated by Leuthold et al., 2012) was used to calculate  $\epsilon_{\text{Hf}(t)}$  of each single-spot analysis. The calculated  $\epsilon_{\text{Hf}(t)}$  is insensitive to the precise age used, and changes by  $\leq 0.1$  even for differences in age up to  $\pm 5$  Ma.

### 5. RESULTS

#### 5.1. Solution MC-ICPMS

Zircons from six samples from the TPIC and five samples from the Chaltén plutonic complex were analyzed by solution MC-ICPMS. Data for single zircons are plotted in Figure 6 and Figure DR8, and given in Table DR1 (see footnote 1).

#### TPIC feeder zone (ca. 12.6 Ma)

Four zircons from **JL438** gave a weighted mean  $^{176}\text{Hf}/^{177}\text{Hf}$  of  $0.28282 \pm 0.00004$ , corresponding to an  $\epsilon_{\text{Hf}(t)}$  of  $1.4 \pm 1.4$  (95% confidence). Five zircons from **JL439** gave an indistinguishable weighted mean  $^{176}\text{Hf}/^{177}\text{Hf}$  of  $0.28284 \pm 0.00002$  with  $\epsilon_{\text{Hf}(t)}$  of  $2.2 \pm 0.7$  (Fig. 6).

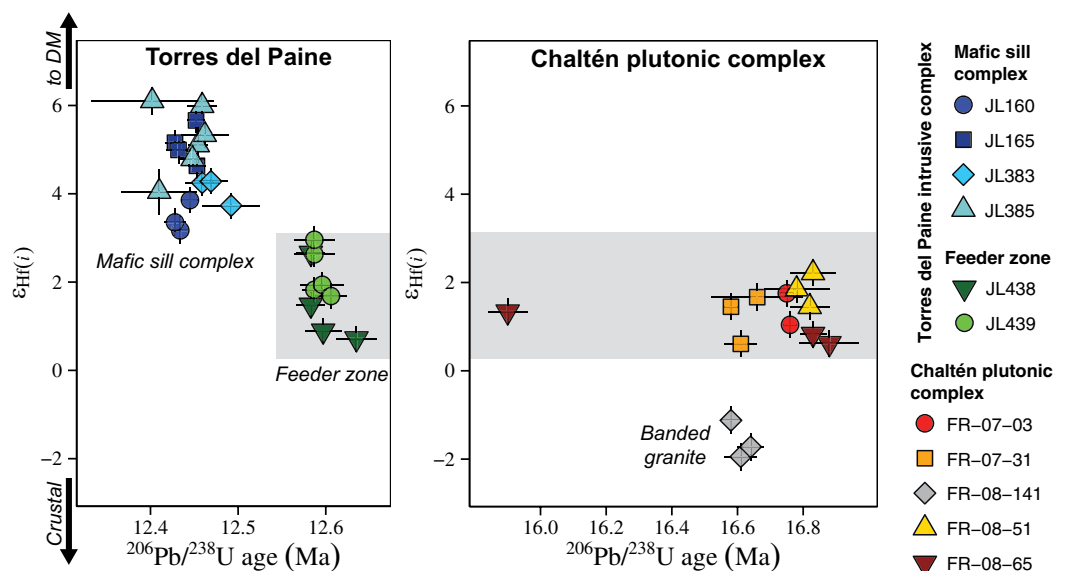
#### TPIC mafic sill complex (ca. 12.45 Ma)

All four mafic sill complex samples have weighted mean  $^{176}\text{Hf}/^{177}\text{Hf}$  and  $\epsilon_{\text{Hf}(t)}$  that are identical within error, but distinctly higher (more radiogenic) than the feeder zone samples (Fig. 6). Three zircons from **JL160** gave a weighted mean  $^{176}\text{Hf}/^{177}\text{Hf}$  of  $0.28288 \pm 0.00001$  and  $\epsilon_{\text{Hf}(t)}$  of  $3.5 \pm 0.4$ . Of five zircon solutions from **JL165**, one was excluded for having significantly higher Yb/Hf and strongly offset  $^{176}\text{Hf}/^{177}\text{Hf}$  from other analyses of the same sample (Fig. DR4A; Table DR1). This raised  $^{176}\text{Hf}/^{177}\text{Hf}$  may reflect an interference from a REE-oxide that only affects high-REE zircons. The remaining four analyses gave a weighted mean  $^{176}\text{Hf}/^{177}\text{Hf}$  of  $0.28292 \pm 0.00002$  and an  $\epsilon_{\text{Hf}(t)}$  of  $5.1 \pm 0.7$ . Three zircons from **JL383** gave a weighted mean  $^{176}\text{Hf}/^{177}\text{Hf}$  of  $0.28289 \pm 0.00001$  and an  $\epsilon_{\text{Hf}(t)}$  of  $4.1 \pm 0.4$ . Six zircons from **JL385** gave a weighted mean  $^{176}\text{Hf}/^{177}\text{Hf}$  of  $0.28293 \pm 0.00002$  and an  $\epsilon_{\text{Hf}(t)}$  of  $5.2 \pm 0.8$ .

#### Chaltén plutonic complex (ca. 16 Ma)

Three zircons from the gabbro-norite **FR-08-51** gave a weighted mean  $^{176}\text{Hf}/^{177}\text{Hf}$  of  $0.28283 \pm 0.00003$  and  $\epsilon_{\text{Hf}(t)}$  of  $1.8 \pm 0.4$  (Fig. 6). Three zircons from gabbro-norite **FR-08-65** gave a weighted mean that is not significantly different with  $^{176}\text{Hf}/^{177}\text{Hf}$  of  $0.28280 \pm 0.00001$  and  $\epsilon_{\text{Hf}(t)}$  of  $0.9 \pm 0.4$ . Three zircons from granodiorite **FR-07-31** gave an indistinguishable weighted mean  $^{176}\text{Hf}/^{177}\text{Hf}$  of  $0.28281 \pm 0.00004$  and an  $\epsilon_{\text{Hf}(t)}$  of  $1.2 \pm 1.4$ . For the tonalite **FR-07-03**, two of four analyzed zircons had high Lu/Hf and Yb/Hf (Table DR1) and gave much higher  $^{176}\text{Hf}/^{177}\text{Hf}$  values, well outside of error, than the other two zircons from this sample. These outlier  $^{176}\text{Hf}/^{177}\text{Hf}$  values show a strong correlation with  $^{176}\text{Lu}/^{177}\text{Hf}$  and  $^{173}\text{Yb}/^{177}\text{Hf}$  (Fig. DR4B). They are attributed to either inadequate correction of isobaric Yb and Lu interferences at high REE/Hf, or the appearance of GdO interferences at these higher values of REE/Hf; these two analyses are excluded. The remaining two zircons from **FR-07-03** gave a weighted mean indistinguishable from the other samples with  $^{176}\text{Hf}/^{177}\text{Hf}$  of  $0.28282 \pm 0.00001$  ( $2\sigma$ ) and  $\epsilon_{\text{Hf}(t)}$  of  $1.4 \pm 0.5$  ( $2\sigma$ ). Quoted errors are  $2\sigma$  internal for this sample only, as with only two analyses the 95% confidence errors calculated by Isoplot (which incorporates a  $1\sigma$  factor for small populations) became unreasonably large. The granite **FR-08-141** has a resolvably less radiogenic Hf

**Figure 6.** Initial  $\epsilon_{\text{Hf}}$  measured for single zircons from eleven samples by solution multi-collector–inductively coupled plasma–mass spectrometer, plotted against published age for the same zircon from Leuthold et al. (2012) or Ramírez de Arellano et al. (2012). Note that the errors plotted here are probably underestimated, as the propagated session reproducibility is for a Yb-free solution; a more realistic reproducibility for our Yb-bearing zircons is  $\sim 0.7$   $\epsilon_{\text{Hf}}$ -units (see Section 4.1). Any apparent intra-sample variability is therefore not interpreted as significant. Samples analyzed from the mafic sill complex were diorites and hornblende gabbros; from the feeder zone, pegmatitic segregations in gabbro-norite; and from the Chaltén complex, lithologies ranging from gabbro-norite to granite (Table 1). Black arrows on left indicate the direction of increasingly crustal Hf isotope compositions and of the depleted mantle (DM), respectively. Note that plots for the Torres del Paine intrusive complex (TPIC) (left) and Chaltén plutonic complex (right) have the same scale on their y-axes (but different scales for their x-axes). Gray box highlights the consistent Hf isotope composition from the ca. 17 Ma Chaltén plutonic complex to the ca. 12.5 Ma TPIC.  $^{176}\text{Hf}/^{177}\text{Hf}$  of single zircon solution analyses is plotted in Figure DR8 (see footnote 1).



isotope composition than the four other Chaltén plutonic complex samples, with weighted mean  $^{176}\text{Hf}/^{177}\text{Hf}$  of  $0.28273 \pm 0.00003$  and  $\epsilon_{\text{Hf}(i)}$  of  $-1.6 \pm 1.1$  (Fig. 6).

## 5.2. Laser Ablation MC-ICPMS

Zircons from thirteen samples (TPIC granites and small intrusions and dikes in the Torres del Paine area) were analyzed by LA-MC-ICPMS (Fig. 7; Table 2; Table DR2; see footnote 1). Zircons are simple in CL, and almost never show evidence for multiple domains indicating more than one generation of growth (Fig. 4). Discordant central domains suggestive of inherited cores were observed only in one or two grains from a few samples (Fig. 4F).

From a total of 161 analyses in six LA-MC-ICPMS sessions, six analyses that were extremely short or sampled inclusions visible in post-analysis inspection gave no part with reliable  $^{176}\text{Hf}/^{177}\text{Hf}$  and were discarded a priori (not plotted). Other analyses that were excluded are identified in gray in Figure 7 and Table DR2, due to: unsuccessful correction of mass bias identified by anomalous  $^{178}\text{Hf}/^{177}\text{Hf}$ ,  $^{173}\text{Yb}/^{177}\text{Hf}$  above that of the highest-Yb standard that was accurate in the same session, either rapidly drilling through the zircon or dramatic zoning in Yb, Hf, or Ta contents, if these were associated with outlier  $^{176}\text{Hf}/^{177}\text{Hf}$ . Note that “outlier” analyses were not excluded only for being outliers, without independent evidence indicating that they may be analytically compromised. Most of the samples have weighted mean  $\epsilon_{\text{Hf}(i)}$  with mean square of weighted deviates (MSWDs) in the range of  $\sim 1$  to 2 (Table 2) indicating that acceptable analyses of zircons from each sample define a single, homogeneous population.

### ca. 30 Ma Alkaline Gabbro

**11-TPM-73A** was analytically challenging because its zircons have extremely high REE contents. They have Gd/Hf up to 15 times higher than zircons from other samples (Manzini, 2012), and up to six times higher than that of MUN-4 (data of Fisher et al., 2011). This sample was analyzed in two sessions. In the first, the Yb interference was not successfully corrected at high  $^{173}\text{Yb}/^{177}\text{Hf}$  ( $\geq 0.2$ ; Fig. DR3; see footnote 1). All analyses with  $^{173}\text{Yb}/^{177}\text{Hf}$   $\geq 0.2$  from this session were excluded, leaving only two analyses of 11-TPM-73A. In the second session, three analyses of 11-TPM-73A were excluded because they had significantly higher  $^{173}\text{Yb}/^{177}\text{Hf}$  than the highest-Yb standard (MUN-4) and higher  $^{176}\text{Hf}/^{177}\text{Hf}$  than the rest of the population. Five other analyses with outlier high  $^{176}\text{Hf}/^{177}\text{Hf}$  attributed to a Gd-oxide interference were excluded. Gd is the principal source

of isobaric interferences from REE oxides, including on our instrument (D’Abzac et al., 2016), owing to its relatively high oxide production rate (Payne et al., 2013). There is a general trend of higher  $^{176}\text{Hf}/^{177}\text{Hf}$  at higher Gd/Hf for 11-TPM-73A zircons for which trace element data exist (data of Manzini, 2012). Pooling the seven acceptable analyses of 11-TPM-73A from two sessions, which are indistinguishable, gives  $^{176}\text{Hf}/^{177}\text{Hf}$  of  $0.282921 \pm 0.000039$  and an  $\epsilon_{\text{Hf}(i)}$  of  $5.4 \pm 1.4$  for its age of ca. 30 Ma.

### ca. 16 Ma Calc-Alkaline Intrusions

The ca. 16 Ma calc-alkaline intrusions all have similar  $\epsilon_{\text{Hf}(i)}$  clustered in the range of  $-1$  to  $+2$ , but scattered slightly outside of error (Fig. 8). A granodiorite from the Olvidado complex (**13-OLV-1**; Fig. 2A) has the most radiogenic  $^{176}\text{Hf}/^{177}\text{Hf}$  at  $0.282836 \pm 0.000010$ , corresponding to an  $\epsilon_{\text{Hf}(i)}$  of  $2.2 \pm 0.4$  (Figs. 7 and 8). Not included in this population was one inherited core, visible in CL and dated to  $>2700$  Ma (Müntener et al., 2018), which gave a dramatically lower  $\epsilon_{\text{Hf}(16\text{ Ma})}$  of  $-67 \pm 1$  for the first part of the analysis ( $\epsilon_{\text{Hf}(2700\text{ Ma})}$  of  $-9 \pm 1$ ; Fig. 7; Table DR2; Fig. DR9; see footnote 1). The second part of this analysis drilled through the core domain and into the underlying rim, and gave  $\epsilon_{\text{Hf}(16\text{ Ma})}$  of  $2.2 \pm 1.7$  (Fig. DR9), which was included in the main population.

Gabbro **11-TPM-61A** has  $^{176}\text{Hf}/^{177}\text{Hf}$  of  $0.282817 \pm 0.000009$  and  $\epsilon_{\text{Hf}(i)}$  of  $1.5 \pm 0.3$ . The **13-TP2-1** granodiorite has  $^{176}\text{Hf}/^{177}\text{Hf}$  within error at  $0.282798 \pm 0.000013$ , and an  $\epsilon_{\text{Hf}(i)}$  of  $0.8 \pm 0.4$ . Granitic pegmatite **PP-36** has indistinguishable  $^{176}\text{Hf}/^{177}\text{Hf}$  of  $0.282786 \pm 0.000010$  and  $\epsilon_{\text{Hf}(i)}$  of  $0.4 \pm 0.3$  (Fig. 8). Two analyses of core domains from granite **09-PR-06** gave distinctly low  $\epsilon_{\text{Hf}(16\text{ Ma})}$  of  $-33 \pm 1$  and  $-8 \pm 1$  (Fig. 7; Table DR2), and were excluded from the magmatic population. These cores are interpreted as inherited based on, respectively, a concordant age of  $565 \pm 5$  Ma (Müntener et al., 2018), and clearly discordant and partially resorbed character in CL (Fig. 4F).  $^{176}\text{Hf}/^{177}\text{Hf}$  of the **09-PR-06** magmatic population was determined from seven analyses as  $0.282770 \pm 0.000011$ , giving an  $\epsilon_{\text{Hf}(i)}$  of  $-0.2 \pm 0.4$ . This weighted mean excluded three analyses with excess scatter attributed to transient instrumental instability, noting that their exclusion makes a negligible difference ( $0.2 \epsilon_{\text{Hf}}$ -units) to the calculated weighted mean  $^{176}\text{Hf}/^{177}\text{Hf}$ . The granodiorite **JL204** has the lowest  $^{176}\text{Hf}/^{177}\text{Hf}$  of  $0.282759 \pm 0.000008$ , and  $\epsilon_{\text{Hf}(i)}$  of  $-0.6 \pm 0.3$  (Figs. 7 and 8).

### TPIC Granites (12.5–12.6 Ma)

A sample of Granite III, **JM-04-66**, gave  $^{176}\text{Hf}/^{177}\text{Hf}$  of  $0.282793 \pm 0.000009$  and  $\epsilon_{\text{Hf}(i)}$  of  $0.6 \pm 0.3$  (Fig. 7), lower than the main range

recorded by zircons from mafic feeder zone samples (Fig. 8). Two samples from Granite I, **JM-05-80** and **JM-05-77**, gave indistinguishable  $^{176}\text{Hf}/^{177}\text{Hf}$  of  $0.282841 \pm 0.000015$  and  $0.282839 \pm 0.000013$ . These samples have  $\epsilon_{\text{Hf}(i)}$  of  $2.3 \pm 0.5$  and  $2.2 \pm 0.5$ , respectively (Fig. 7), indistinguishable from the two mafic samples from the feeder zone (Fig. 8).

### ca. 12 Ma Dikes and Small Intrusions

The ca. 12 Ma dikes and small intrusion external to the TPIC all have indistinguishable  $\epsilon_{\text{Hf}(i)}$  (Fig. 8). **11-TPM-32A** gave  $^{176}\text{Hf}/^{177}\text{Hf}$  of  $0.282845 \pm 0.000016$  and  $\epsilon_{\text{Hf}(i)}$  of  $2.4 \pm 0.6$  (Fig. 7). **11-TPM-85** gave  $^{176}\text{Hf}/^{177}\text{Hf}$  of  $0.282851 \pm 0.000014$  and  $\epsilon_{\text{Hf}(i)}$  of  $2.6 \pm 0.5$ . **11-TPM-94** gave a weighted mean  $^{176}\text{Hf}/^{177}\text{Hf}$  of  $0.282861 \pm 0.000016$  and  $\epsilon_{\text{Hf}(i)}$  of  $3.0 \pm 0.6$  (Fig. 7).

## 6. DISCUSSION

### 6.1. Relationship between Granitic and Mafic Units of the TPIC

The two TPIC granite units analyzed (Granites I and III) have distinct Hf isotope compositions, and Granite III shows a slightly more crustal signature (Fig. 8). Published whole rock Nd isotope data for the TPIC show the same trend, although the two granite units are indistinguishable in terms of whole rock Sr isotopes (Leuthold et al., 2013).

Both granite units have  $\epsilon_{\text{Hf}(i)}$  that falls within the range of the feeder zone, and is distinctly lower than any sample from the mafic sill complex (Fig. 8). Although Granite I crops out only above the mafic sill complex and is not observed in the feeder zone, Leuthold et al. (2013) concluded that mafic rocks from the feeder zone (or their equivalents at depth) are the complementary cumulates to Granite I, based on their indistinguishable U–Pb ages, as well as geochemical and isotopic modeling and field observations. This conclusion is unequivocally supported by our Hf isotope results, given the indistinguishable  $\epsilon_{\text{Hf}(i)}$  for all Granite I and feeder zone gabbro samples. Granite III outcrops in both the feeder zone and the sill complex. It has a U–Pb age intermediate between mafic units of the feeder zone and sill complex, although it overlaps in age with the oldest unit of the mafic sill complex (Leuthold et al., 2012). However, based on geochemical modeling, Leuthold et al. (2013) argued that there is no genetic link between the mafic sill complex and Granite III. Our Hf isotope data support this conclusion and provide evidence that Granite III was also derived from mafic cumulates related to the feeder zone and not the sill complex.

## Rapidly changing mantle sources in the south Patagonian retro-arc

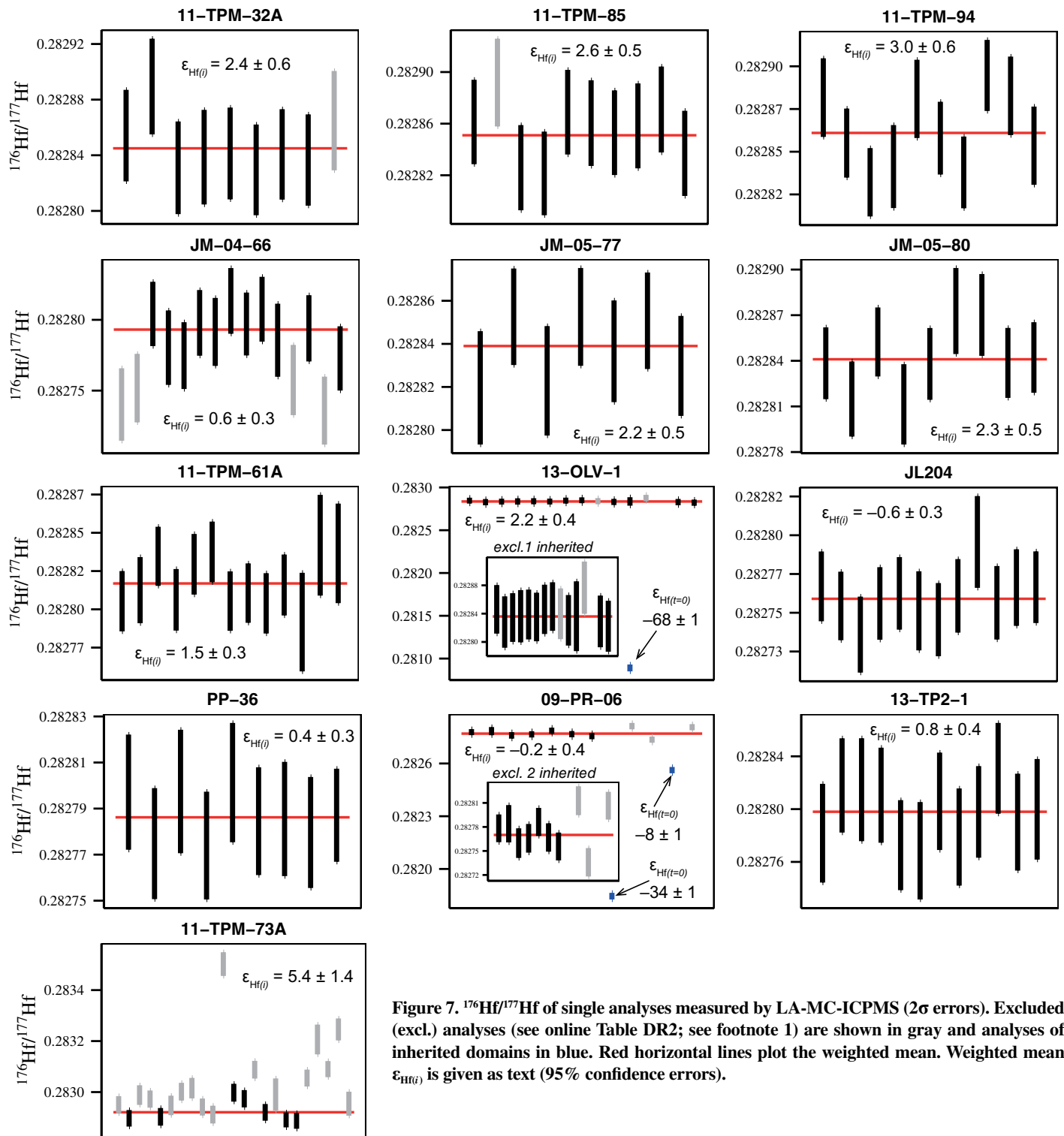


**Figure 7.**  $^{176}\text{Hf}/^{177}\text{Hf}$  of single analyses measured by LA-MC-ICPMS ( $2\sigma$  errors). Excluded (excl.) analyses (see online Table DR2; see footnote 1) are shown in gray and analyses of inherited domains in blue. Red horizontal lines plot the weighted mean. Weighted mean  $\epsilon_{\text{Hf}(t)}$  is given as text (95% confidence errors).

## 6.2. Isotopically Enriched South Patagonian Sub-Continental Mantle

In oceanic arcs, back-arc magmatic rocks can be used to constrain the Hf isotopic composition of “ambient mantle” for a given arc, prior to the imprinting of any subduction sig-

nature (Woodhead et al., 2012). Similarly, the Hf isotopic composition of retro-arc magmatic rocks in a continental arc may give insight into the nature of the ambient mantle, as long as they did not experience crustal assimilation. The ca. 30 Ma Amarga alkaline gabbro has OIB-like trace element chemistry, similar to

alkaline plateau basalts erupted in the South Patagonian retro-arc to the east (Espinoza et al., 2005; Guivel et al., 2006; Müntener et al., 2018) (Figs. 9 and 10). Its alkaline nature, OIB-like trace element chemistry, and the absence of the trace element enrichments (e.g., Th, Pb) and depletions (e.g., Nb, Ti) that characterize

TABLE 2. WEIGHTED AVERAGE  $^{176}\text{Hf}/^{177}\text{Hf}$  AND  $\epsilon_{\text{Hf}(t)}$  OF SAMPLES FROM THE TORRES DEL PAINE AND CHALTÉN REGIONS, PATAGONIA, SOUTH AMERICA, ANALYSED BY SOLUTION OR LASER ABLATION MC-ICPMS

Sample	Lithology	Age (Ma)	Method (Hf)	Wtd. av. $^{176}\text{Hf}/^{177}\text{Hf}$	$\pm$ (95% conf.)*	Wtd. av. $\epsilon_{\text{Hf}(t)}$	$\pm$ (95% conf.)*	MSWD	<i>n</i>
<b>Torres del Paine intrusive complex</b>									
<b>Mafic sill complex</b>									
JL160	Hornblende gabbro	12.434 $\pm$ 0.0009 <sup>1</sup>	Solution	0.28288	0.00001	3.5	0.4	1.0	3/3
JL165	Layered diorite	12.431 $\pm$ 0.0006 <sup>1</sup>	Solution	0.28292	0.00002	5.1	0.7	1.5	4/5
JL383	Hornblende gabbro	12.472 $\pm$ 0.0009 <sup>1</sup>	Solution	0.28289	0.00001	4.1	0.4	0.8	3/3
JL385	Diorite sill	12.453 $\pm$ 0.01 <sup>1</sup>	Solution	0.28293	0.00002	5.2	0.8	4.8	6/6
<b>Feeder zone</b>									
JL438	Gabbro <sup>^</sup>	12.587 $\pm$ 0.009 <sup>1</sup>	Solution	0.28282	0.00004	1.4	1.4	6.2	4/4
JL439	Gabbro <sup>^</sup>	12.593 $\pm$ 0.009 <sup>1</sup>	Solution	0.28284	0.00002	2.2	0.7	2.5	5/5
<b>Granites</b>									
JM-04-66	Granite	12.49 $\pm$ 0.01 <sup>2</sup>	Laser	0.282793	0.000009	0.6	0.3	1.3	11/15
JM-05-80	Granite	12.58 $\pm$ 0.01 <sup>2</sup>	Laser	0.282841	0.000015	2.3	0.5	2.6	9/9
JM-05-77	Granite	12.58 $\pm$ 0.01 <sup>2</sup>	Laser	0.282839	0.000013	2.2	0.5	1.4	7/7
<b>ca. 12 Ma dikes and small intrusions (Torres del Paine region)</b>									
11-TPM-85	Microgranitic dike	12.3 $\pm$ 0.2 <sup>3</sup>	Laser	0.282851	0.000014	2.6	0.5	1.2	9/10
11-TPM-94	Monzonite intrusive	12.4 $\pm$ 0.2 <sup>3</sup>	Laser	0.282861	0.000016	3.0	0.6	4.1	10/10
11-TPM-32A	Bimodal dike	12.8 $\pm$ 0.2 <sup>3</sup>	Laser	0.282845	0.000016	2.4	0.6	1.3	8/9
<b>ca. 16 Ma calc-alkaline intrusions (Torres del Paine region)</b>									
13-OLV-1	Monzogranite	15.7 $\pm$ 0.4 <sup>3</sup>	Laser	0.282836	0.000010	2.2	0.4	0.2	12/15
13-TP2-1	Granodiorite	15.9 $\pm$ 0.4 <sup>3</sup>	Laser	0.282798	0.000013	0.8	0.4	1.2	12/12
09-PR-06	Granite	16.1 $\pm$ 0.2 <sup>3</sup>	Laser	0.282770	0.000011	-0.2	0.4	1.7	7/12
11-TPM-61A	Diorite	16.2 $\pm$ 0.2 <sup>3</sup>	Laser	0.282817	0.000009	1.5	0.3	1.8	13/13
PP-36	Granite	16.4 $\pm$ 0.2 <sup>3</sup>	Laser	0.282786	0.000008	0.4	0.3	0.7	9/9
JL-204	Diorite	16.5 $\pm$ 0.2 <sup>3</sup>	Laser	0.282759	0.000008	-0.6	0.3	1.2	12/12
<b>Chaltén plutonic complex</b>									
FR-08-65	Gabbro <sup>^</sup>	16.83 $\pm$ 0.04 <sup>4</sup>	Solution	0.28280	0.00001	0.9	0.4	1.1	3/3
FR-08-51	Gabbro <sup>^</sup>	16.78 $\pm$ 0.10 <sup>4</sup>	Solution	0.28283	0.00003	1.8	0.4	1.2	3/3
FR-07-03	Tonalite	16.70 $\pm$ 0.06 <sup>4</sup>	Solution	0.28282	0.00001*	1.4	0.5*	2.1	2/4
FR-07-31	Granodiorite	16.58 $\pm$ 0.02 <sup>4</sup>	Solution	0.28281	0.00004	1.2	1.4	2.6	3/3
FR-08-141	Banded granite	16.58 $\pm$ 0.03 <sup>4</sup>	Solution	0.28273	0.00003	-1.6	1.1	1.5	3/3
<b>ca. 30 Ma alkaline gabbro (Torres del Paine region)</b>									
11-TPM-73A	Alkaline gabbro	ca. 30 Ma <sup>3</sup>	Laser	0.282921	0.000039	5.4	1.4	6.8	7/23

Notes: "Method (Hf)" indicates whether Hf isotopes were measured by solution or laser ablation multicollector inductively coupled plasma mass spectrometry (MC-ICPMS). The U–Pb age calculated for each sample by <sup>1</sup>Leuthold et al. (2012), <sup>2</sup>Michel et al. (2008; recalculated by Leuthold et al. [2012]), <sup>3</sup>Müntener et al. (2018), or <sup>4</sup>Ramírez de Arellano et al. (2012) is given in gray for reference. For laser ablation analyses, the sample age was used to calculate  $\epsilon_{\text{Hf}(t)}$  of individual zircons, while for solution analyses, the U–Pb age of the same individual zircon solution (see Leuthold et al., 2012; Ramírez de Arellano et al., 2012) was used for  $\epsilon_{\text{Hf}(t)}$  calculation. The uncertainty on solution analyses was forced to 0.7  $\epsilon_{\text{Hf}}$  units for calculation of weighted means (see text for discussion). Wtd. av.—weighted average; MSWD—mean square of weighted deviates; *n*—number of analyses used in calculation of weighted mean, as a fraction of the total (including rejected analyses and inherited domains).

<sup>^</sup>Pegmatitic segregations.

\*Errors are 95% confidence (conf.) and incorporate  $\tau$  and a propagated error for any scatter outside analytical errors, except for FR-07-03 for which 2 $\sigma$  internal errors are given. With only two analyses, 95% (conf.) errors calculated for this sample were unreasonably large.

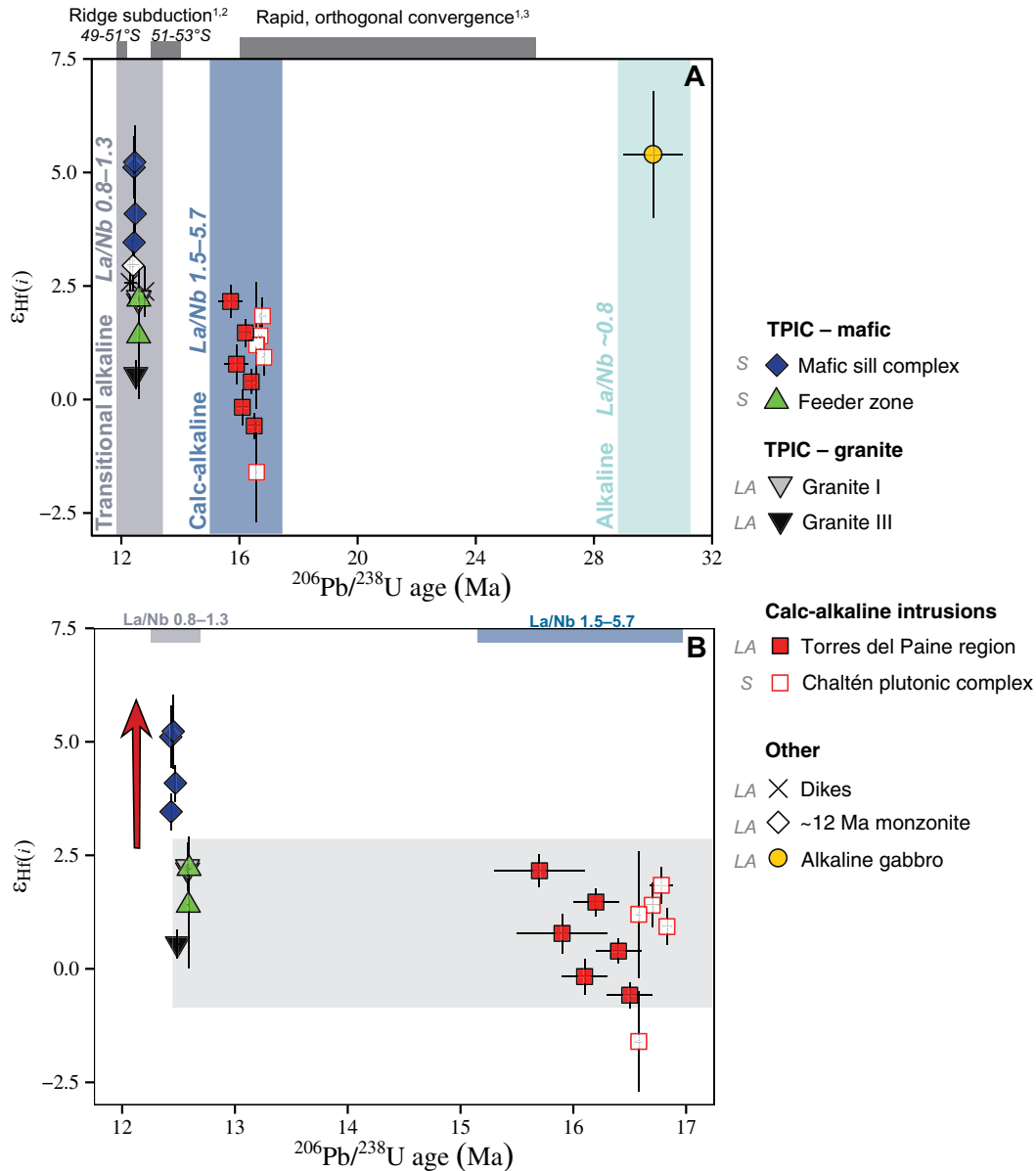
the subduction component (Fig. 10) record low-degree partial melting of retro-arc mantle that had not been fluxed by recent subduction. This petrogenesis is consistent with the fact that the Amarga gabbro was emplaced >60 km inboard of the Patagonian batholith, and well prior to the eastwards migration of arc magmatism at ca. 20–16 Ma (Ramírez de Arellano et al., 2012). The  $\epsilon_{\text{Hf}(t)}$  of  $+5.4 \pm 1.4$  of the Amarga gabbro (Fig. 8; Table 2) therefore represents the "background" Hf isotope composition of the South Patagonian mantle wedge, before it was modified by any modern subduction components. The background  $\epsilon_{\text{Hf}}$  of  $+5.4 \pm 1.4$  is significantly lower than the  $\epsilon_{\text{Hf}}$  of global modern-day depleted mantle (+14 to +18; Vervoort et al., 1999). This low  $\epsilon_{\text{Hf}}$  implies that the unfluxed retro-arc mantle in Patagonia is not pristine depleted mantle, consistent with the continental setting of the arc and evidence from mantle xenoliths for pervasive metasomatism

of the Patagonian back-arc mantle by enriched melts (Rivalenti et al., 2004). The enriched Hf isotope signature has to be inherent to the local sub-continental mantle, and must be an inherited feature (i.e., not related to the contemporaneous subduction), given that the OIB-like trace element chemistry and gabbroic composition of the Amarga gabbro (Müntener et al., 2018; Fig. 9) do not permit any significant contribution from either modern subduction components or assimilated continental crust.

### 6.3. Regional Evolution of the Hf Isotope Composition of Magmatism

A coherent region-wide evolution of  $\epsilon_{\text{Hf}(t)}$  is observed, with three distinct phases. The earliest is recorded by the ca. 30 Ma alkaline gabbro, which has  $\epsilon_{\text{Hf}(t)}$  of  $+5.4 \pm 1.4$  (Fig. 8) and defines the unfluxed retro-arc mantle prior to inboard migration of arc magmatism. The next

phase records distinctly less juvenile Hf isotope compositions, and remarkably consistent  $\epsilon_{\text{Hf}(t)}$  that falls in a narrow band between  $-1$  and  $+3$  from ca. 17–12.5 Ma (Fig. 8). The only notable exception is the Fitzroy banded granite from the Chaltén plutonic complex, which has lower  $\epsilon_{\text{Hf}(t)}$  of  $-1.6 \pm 1.1$  (Figs. 6 and 8; Table 2). This lower  $\epsilon_{\text{Hf}(t)}$  is attributed to assimilation of continental crust having affected the Hf isotope systematics of this granitic magma only. This interpretation is supported by published U–Pb data: of the Chaltén plutonic complex samples we have analyzed, the Fitzroy granite is the only one that contained zircons with ages significantly older than the magmatic age, which were interpreted as xenocytic cores acquired by crustal assimilation (Ramírez de Arellano et al., 2012). The period of consistent  $\epsilon_{\text{Hf}(t)}$  ends abruptly, and a sudden jump to more juvenile  $\epsilon_{\text{Hf}(t)}$  of  $+3.5$ – $5.5$  is recorded by the younger ca. 12.45 Ma mafic sill complex (Figs. 6 and 8). The Hf isotope



composition of these samples is distinct from all 17–12.5 Ma intrusions, but similar to that of the ca. 30 Ma alkaline gabbro.

Two bimodal dikes (11-TPM-32A, 11-TPM-85) and one monzonite from outside the TPIC (11-TPM-94) have ca. 12.5 Ma LA-ICPMS ages that, due to their relatively low precision, are within error of both the mafic sill complex and the feeder zone (Müntener et al., 2018). Although all bimodal dykes observed intersecting the TPIC post-date Granite III, no field relations were observed that directly constrain the relationship of the analyzed samples with the main units (Section DR1). The dikes and monzonite have Hf isotope compositions that are intermediate between the feeder zone and the mafic sill complex, albeit within error of samples from both units. This re-

lationship hints at the possibility that the abrupt shift to more juvenile  $\epsilon_{\text{Hf}(t)}$  may occur as a continuous transition rather than a single jump. However, the ages of these minor intrusions are too imprecise to constrain how they relate temporally to the main units of the TPIC, and they have ages that could fall on either side of the major shift in Hf isotope composition observed within the TPIC. Because of this uncertainty, these samples will not be considered further in the regional Hf isotope evolution. A critical observation is that whether the shift in  $\epsilon_{\text{Hf}(t)}$  occurred gradually or in a single jump, it must have occurred on very short timescales ( $<20 \pm 10$  k.y.).

All of the analyzed zircon samples have somewhat enriched Hf isotope compositions, with  $\epsilon_{\text{Hf}(t)}$  significantly lower than the modern

depleted mantle. Magmas derived directly from the isotopically enriched local subcontinental mantle (Section 6.2), with no addition of a crustal component, would be expected to share its enriched Hf isotope composition ( $\epsilon_{\text{Hf}}$  of  $+5.4 \pm 1.4$ ). However, 17–12.5 Ma magmas have resolvable lower  $\epsilon_{\text{Hf}(t)}$  than this ambient mantle, indicating that over this time period there was input of an additional continental crustal component to melts of the already inherently enriched local mantle. This additional crustal component is absent from the ca. 12.45 Ma mafic sill complex samples. In the following sections, the origin of the additional crustal component recorded from ca. 17 to 12.5 Ma, and the cause of its rapid ( $<20 \pm 10$  k.y.) disappearance by ca. 12.45 Ma, will be explored.

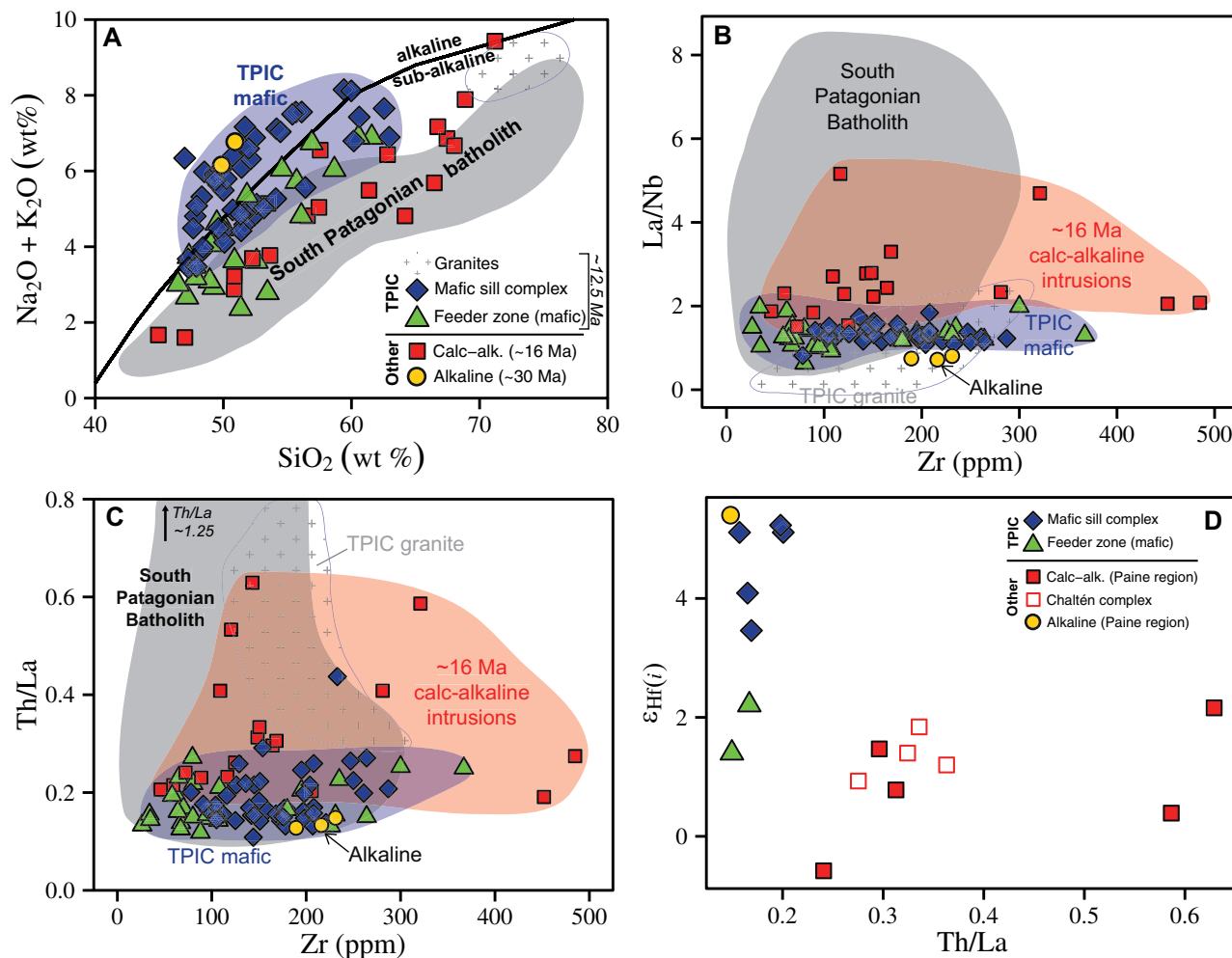


**Figure 9.** (A–C) Published whole rock geochemical data for the mafic Torres del Paine intrusive complex (TPIC) (Leuthold et al., 2013) and calc-alkaline and alkaline intrusions from the Torres del Paine region (Müntener et al., 2018). Fields with crosses delineate whole rock data for Torres del Paine granites (Michael, 1984). Gray fields show the range for the South Patagonian batholith (Hervé et al., 2007). (A) Total alkali versus silica diagram. Alkaline–sub-alkaline boundary of Irvine and Baragar (1971). The blue field highlights mafic rocks of the TPIC (both mafic sill complex and feeder zone) with  $\text{Eu}^*/\text{Eu} \leq 1.0$ , thus excluding the most strongly cumulate samples. (B, C) La/Nb and Th/La plotted against Zr, used as a measure of degree of differentiation. TPIC and alkaline intrusions show less subduction influence from slab components (as tracked by La/Nb) and subducted continental crust and/or sediments (Th/La) than calc-alkaline intrusions and the batholith, at all degrees of differentiation. (D)  $\epsilon_{\text{Hf}(i)}$  of zircon versus whole rock Th/La for units analyzed for Hf isotopes; whole rock data for Chaltén plutonic complex from Ramírez de Arellano et al. (2012). For four TPIC samples, whole rock data for the same sample analyzed were not available. Either an equivalent sample collected from the same locality was used (mafic sill complex), or the average of all analyses of the same lithology (feeder zone). TPIC granites are not plotted, as published whole rock data do not distinguish which granite units samples came from. Note the lack of systematic relationship between  $\epsilon_{\text{Hf}(i)}$  and Th/La, and thus the subducted sediment contribution.  $\epsilon_{\text{Hf}(i)}$  vs La/Nb shows identical behavior (Fig. DR13; see footnote 1).

#### 6.4. Origin of the Increased Crustal Contribution 17–12.5 Ma

There are several possible origins for the additional crustal component identified in 17–12.5 Ma plutonic rocks. One possibility is that their source magmas were extracted from “background” subcontinental mantle, then assimilated some continental crust on transport through, storage in, or final emplacement in the

crust. An alternative possibility is that addition of the crustal component occurred in the mantle wedge itself, prior to mantle melting, and the partial melts extracted from this recently re-enriched mantle experienced little or no crustal assimilation during their passage through the continental crust. It is well established that crustal Hf isotope signatures can be transferred to arc magmas through the mantle wedge by partial melting of subducted continental compo-

nents, either sediments or eroded forearc continental crust (e.g., Nebel et al., 2011; Ranero and von Huene, 2000; Straub et al., 2015).

The remarkable consistency of the Hf isotope composition of 17–12.5 Ma intrusions argues against any significant addition of a crustal Hf component by assimilation of continental crust into these separate magma chambers during ascent or emplacement, except for the Fitzroy banded granite (Section 6.3). The period

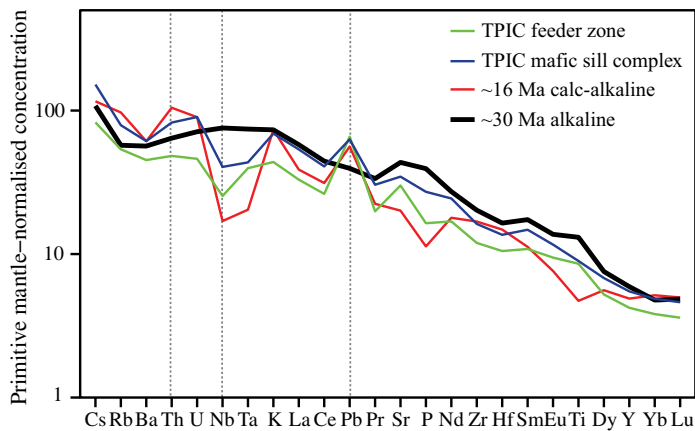


**Figure 10. Multi-element plot of averaged whole rock geochemical data for the Torres del Paine intrusive complex (TPIC) feeder zone and mafic sill complex plutonic units (data from Leuthold et al., 2013), and the ca. 16 Ma calc-alkaline and ca. 30 Ma alkaline intrusions in the Torres del Paine region (data from Müntener et al., 2018). Concentrations are normalized to the primitive mantle values of McDonough and Sun (1995). Gray dashed lines highlight some elements that record a subduction component.**

The striking paucity of inherited zircon in even the most evolved intrusions supports our conclusion that crustal assimilation within the crust was limited, and did not produce the crustal Hf signature. Zircons rarely showed evidence in CL images for discordant central domains that resemble inherited cores (Fig. 4), and we deliberately targeted all such domains observed. Nonetheless, only three analyses from two evolved ca. 16 Ma intrusions, out of a total of 155 LA-MC-ICPMS analyses from 13 samples, gave Hf isotope compositions distinct from the magmatic population in the same sample (Fig. 7). These analyses had extremely unradiogenic  $\epsilon_{\text{Hf}(16 \text{ Ma})}$  of  $-8$ ,  $-33$ , and  $-67$ , and ancient U–Pb ages of 550–2700 Ma (Müntener et al., 2018). The presence of rare inherited cores in these two intrusions is attributed to assimilation of a small quantity of Paleozoic metasedimentary units, which are known to include ancient zircons (Hervé et al., 2003). Although a Paleozoic metamorphic basement has been assumed to underlie the Torres del Paine region (e.g., Fosdick et al., 2011), these inherited zircons provide the first direct evidence for it. The fact that even in the two samples with inherited cores, these were rare, suggests only very limited crustal assimilation. That the assimilation they record had little effect on the Hf isotope composition is evident from the fact that 13-OLV-1 has an inherited core with  $\epsilon_{\text{Hf}(16 \text{ Ma})}$  of  $-67$ , but still has the most radiogenic (least crustal) magmatic  $\epsilon_{\text{Hf}(t)}$  of the calc-alkaline intrusions (Table 2). The complete absence of inherited zircons in the 11 other samples analyzed by LA-MC-ICPMS testifies to a generalized lack of crustal assimilation.

Altogether, the consistent Hf isotope signature over  $>4$  m.y. and  $\sim 200$  km favors addition of a crustal component in the mantle wedge, which can easily explain the consistent low  $\epsilon_{\text{Hf}(t)}$  of all magmas from 17 to 12.5 Ma. The continent-wards migration of arc magmatism from 20 to 16 Ma was associated with a period of intense subduction erosion at  $\sim 48$ – $51^\circ\text{S}$ , which removed  $\sim 180$  km of forearc crust (Ramírez de Arellano et al., 2012; Thomson et al., 2001). The forearc crust eroded during this subduction erosion could be the source of the crustal component introduced into the mantle wedge and recorded in the Hf isotope composition of 17–12.5 Ma magmas. Subducted sediments are another potential source, but the exposed surface lithologies south of  $47^\circ\text{S}$  favor eroded forearc crust as the source of the mantle contaminant. There are no direct constraints on the Hf isotope composition of sediments in the forearc accretionary prism at these latitudes, but these are expected to be dominated by terrigenous detritus derived from the exposed part of the

of stable  $\epsilon_{\text{Hf}(t)}$  spans  $>4$  m.y., and includes diverse intrusions: various 17–16 Ma calc-alkaline intrusions in the Torres del Paine region, the Chaltén plutonic complex  $\sim 200$  km to the north, mafic lithologies from the oldest part of the TPIC (the feeder zone), and Granites I and III from the TPIC. It would require a remarkable degree of coincidence to achieve such a homogenous Hf isotope composition on such large temporal and spatial scales (17–12.5 Ma and  $\sim 200$  km) by crustal assimilation in numerous separate magma chambers. This conclusion is supported by the fact that the calc-alkaline intrusions from both Chaltén and Torres del Paine regions range from gabbro-norite to granite in composition, but all intrusions have similar  $\epsilon_{\text{Hf}(t)}$  from the most primitive to the most evolved lithologies, and across a wide range in bulk rock  $\text{SiO}_2$  (Figs. DR10, DR11; see footnote 1). If assimilation in the crust were the dominant source of the crustal Hf component, more primitive compositions would be expected to record less crustal influence than more evolved compositions, as the latter would have had more opportunity to ingest continental crust during fractionation and the associated residence in the crust.

We note that although we can rule out assimilation within the crust as the origin of the crustal Hf component in 17–12.5 Ma magmas, our data do *not* rule out any crustal assimilation having occurred at all. Previous work showed that TPIC magmas were not transported directly from mantle/lower crustal source reservoirs to be emplaced immediately into shallow crustal levels. Rather, microtextural evidence

and thermobarometry of hornblende cores indicate that some differentiation of TPIC magmas occurred in middle crustal reservoirs prior to their emplacement at shallow crustal levels (Leuthold et al., 2014). There is also evidence for a small amount of crustal assimilation affecting some lithologies from the TPIC feeder zone, in the form of rare marl and quartzite xenoliths in gabbro-norites, which also have slightly more crustal whole rock Nd and Sr isotope signatures (Leuthold et al., 2013). Although our Hf isotope data show no evidence for assimilation within the crust, instead directly recording the mantle source, they do not contradict the previous evidence for residence and fractionation of magmas in a middle crustal chamber with a small degree of assimilation. The long half-life of  $^{176}\text{Lu}$  (ca. 54 Ga; Söderlund et al., 2004) means that extremely long periods of time are required for crust to acquire significantly less radiogenic  $\epsilon_{\text{Hf}}$ . Assimilation of young crust, or lithologies poor in Hf-bearing phases, is therefore not expected to change the Hf isotope composition of magmas. The important point for our study is that, whatever crustal assimilation occurred, it cannot be the origin of the remarkably consistent crustal contribution seen in 17–12.5 Ma magmas, which instead records addition of a significant subducted continental crustal component to the mantle. In this case, the Hf isotope system allows us to “see through” any small amount of assimilation within the crust, recording isotopic changes in the original source composition during ongoing extraction of melts from the mantle.



adjacent continent. South of  $\sim 47^\circ\text{S}$ , surface exposure seaward of the main divide of the Andes is overwhelmingly dominated by Jurassic–Neogene arc magmatic products of the South Patagonian batholith (Hervé et al., 2007). These young igneous units would not have strongly crustal Hf isotope compositions (see Section DR3; see footnote 1). Subducted sediments will have Hf isotope compositions dominated by the overall rather juvenile Patagonian batholith, and are therefore unlikely to represent the crustal contaminant in the mantle. In contrast, eroded forearc crust comes from mechanical erosion of the part of the crust closest to the trench (Ranero and von Huene, 2000), which may include lower crust and/or lithologies not exposed at the surface. The most likely source of crust with highly unradiogenic Hf isotope signatures, suitable to represent the contaminant of the mantle wedge, is Paleozoic to Mesozoic metamorphic complexes with significant proportions of  $>500$  Ma zircons that can have extremely low  $\epsilon_{\text{Hf}(t)}$  (Augustsson et al., 2006; Hervé et al., 2003). Such units (reviewed in detail in Section DR3) are extensively exposed north of  $47^\circ\text{S}$  (Hervé et al., 2003), and are inferred to form the middle and lower crust beneath the Torres del Paine region (Fosdick et al., 2011; see their fig. 3), but crop out only sporadically at the surface at the latitudes of Torres del Paine and El Chaltén. Subduction erosion of forearc crust comprising Paleozoic metasedimentary basement is therefore the most likely mechanism to introduce a strongly crustal component into the subarc mantle.

The situation at  $49\text{--}51^\circ\text{S}$  contrasts to the central Andes ( $28\text{--}32^\circ\text{S}$ ), where the Hf isotope compositions of arc magmas were found to be controlled mainly by assimilation in the crust, with little influence from addition of continental crust to the mantle by subduction erosion (Jones et al., 2015). The dominance of within-crust assimilation in the central Andes, and its near absence in southern Patagonia, could partly result from differences in crustal thickness. The present day crustal thickness is significantly less in Patagonia ( $\sim 30$  km) than in the central Andes ( $\sim 60$  km) (Assumpção et al., 2013; Lawrence and Wiens, 2004; Robertson Maurice et al., 2003), although the Patagonian crust may have been considerably thicker at 17 Ma, after which occurred a period of extension, uplift, and erosion (Boutonnet et al., 2010; Fosdick et al., 2013; Lagabriele et al., 2007; Lagabriele et al., 2004; Thomson et al., 2010). The presence of ancient (Grenville-aged, i.e., 1200–1000 Ma) basement in the central Andes, but not in Patagonia (Jones et al., 2015; Ramos, 2010), may also contribute to the stronger control of crustal assimilation on the Hf isotope composition of

magmatism in the central Andes. The extremely long timescales required to evolve a strongly crustal Hf isotope signature mean that assimilation of relatively young crust such as that found in Patagonia will have much less potential to change  $\epsilon_{\text{Hf}(t)}$  than assimilation of the same quantity of ancient Grenville-aged crust.

### 6.5. Rapid Rejuvenation during Emplacement of the TPIC

One of the most exciting observations from our data is the abrupt shift toward more juvenile Hf isotope compositions within the TPIC (Figs. 6 and 8), from the more crustal signatures of the  $12.593 \pm 0.009$  Ma to  $12.49 \pm 0.02$  Ma feeder zone mafic units and Granites I and III, to the more mantle-like signature of the  $12.472 \pm 0.009$  Ma to  $12.431 \pm 0.006$  Ma mafic sill complex (ages from Leuthold et al., 2012; Michel et al., 2008). Our results thus demonstrate that within this single sheeted magmatic complex, different batches of magma tapped different geochemical reservoirs, in spite of the very short timescales on which the complex was built up ( $162 \pm 11$  ka; Leuthold et al., 2012). The timing of the abrupt shift in Hf isotope composition is bracketed between the youngest granite at  $12.49 \pm 0.01$  Ma and the oldest mafic sill complex unit at  $12.472 \pm 0.009$  Ma (Leuthold et al., 2012; Fig. 7; Michel et al., 2008), constraining the shift to have occurred within  $20 \pm 10$  k.y. The fact that the younger mafic sill complex has more juvenile  $\epsilon_{\text{Hf}(t)}$  demands the input of new primitive melts into the system at this time.

We can exclude late-stage crustal contamination in the feeder zone as the cause of its more crustal  $\epsilon_{\text{Hf}(t)}$  compared to the younger mafic sill complex. It has already been argued that differences in Hf isotope composition in our samples cannot be the result of different degrees of crustal assimilation in the crust (Section 6.4). Late-stage assimilation can particularly be ruled out, as thermal constraints mean that it is not expected to be effective at the shallow levels of emplacement (Thompson et al., 2002). The rare marl and quartzite xenoliths that are observed in some feeder zone units (Section 6.4) do not correspond well lithologically with the surrounding country rock, which is dominantly Late Cretaceous–Tertiary turbidites, sandstone, and shale (e.g., Fosdick et al., 2011; Ghiglione et al., 2016; Wilson, 1991). The xenoliths are commonly stretched and folded (Leuthold et al., 2013). These observations support an origin at greater depth and provide further evidence that the small degree of assimilation the xenoliths record cannot have been late stage. The Hf isotope data therefore unequivocally record a rejuvenation event.

Although Hf isotope data provide the clearest evidence for rapid rejuvenation at ca. 12.45 Ma, this shift is also corroborated by other trace element and isotopic signatures. Whole rock Nd and Sr isotopes show generally more primitive isotopic compositions for the mafic sill complex than the feeder zone (Leuthold et al., 2013), although this trend is complicated by more crustal signatures in Sr isotopes than Nd isotopes for some samples. This difference could result from the more mobile nature of Sr compared to Nd (Rollinson, 1993), making the Sr isotopes more susceptible to post-magmatic modification than Nd (and Hf) isotopes. Olivine from the mafic sill complex has distinctly more primitive compositions than feeder zone olivine, with much higher Ni and Mg contents (Leuthold et al., 2014). Input of new, less-differentiated mantle melts at ca. 12.45 Ma is required to explain these compositions. Established crystallization sequences for all mafic sill complex units show olivine was an early crystallizing phase, and hornblende barometry constrains crystallization of these early minerals to have occurred at mid-crustal depths prior to emplacement of the TPIC at shallower crustal levels (Leuthold et al., 2014). The more evolved composition of feeder zone olivines therefore cannot be explained by emplacement-level assimilation.

#### 6.5.1. Nature of the Rapid Rejuvenation Event

A marked shift in chemistry from calc-alkaline for the 17–16 Ma intrusions, to transitional alkaline for the ca. 12.5 Ma TPIC is recorded by both major and trace element whole rock data (Figs. 9 and 10; Fig. DR12; see footnote 1). Hf isotope composition remains remarkably constant across this major geochemical shift (Fig. 8). Conversely, there is no systematic change in whole rock geochemistry associated with the abrupt shift in Hf isotope composition within the TPIC, which has transitional alkaline chemistry both in the feeder zone and the sill complex (Fig. 9). This decoupling is evident on plots of  $\epsilon_{\text{Hf}(t)}$  against trace element ratios that track subduction influence (e.g., Th/La, La/Nb, Th/Nb), which remain constant across the change in  $\epsilon_{\text{Hf}(t)}$  (Fig. 9D; Fig. DR13; see footnote 1).

The calc-alkaline chemistry of the 17–16 Ma intrusions in the Torres del Paine and Chaltén areas is typical of subduction-related magmatism and has been interpreted as recording the migration of arc magmatism continent-wards (i.e., into the former retro-arc) during a period of fast convergence and subduction erosion from ca. 20–16 Ma (Müntener et al., 2018; Ramírez de Arellano et al., 2012). The transitional alkaline chemistry of the TPIC reflects a change in melting regime compared to the preceding arc

magmatism in this region. The higher incompatible element concentrations (e.g., K, Rb, La; Fig. 10) of TPIC parental magmas imply a low degree of mantle partial melting. An important implication of this observation is that TPIC magmas must have originated from renewed extraction of mantle melts, with lower degrees of partial melting, at ca. 12.6 Ma. They cannot have been derived from a new episode of extraction of magma already stored in the crust, which would be unable to produce the observed transitional alkaline chemistry. This in turn implies that the abrupt shift in Hf isotope composition recorded during the emplacement of the TPIC cannot simply result from a small input of new mantle-derived melts into a pre-existing crustal chamber. Rather, the whole rock chemistry and Hf isotope data together require that at ca. 12.6 Ma, new lower-degree partial melts were extracted from a mantle with the same isotopic composition as that from which the ca. 16 Ma calc-alkaline magmas were produced; and that subsequently, at ca. 12.45 Ma, new low-degree partial melts of mantle with a distinct, more depleted Hf isotope composition were extracted to form the mafic sill complex. The rapid rejuvenation observed at ca. 12.45 Ma in the TPIC must therefore record input of new, more juvenile *mantle-derived* melts during the build-up of this intrusive complex. Input of new mantle-derived melts is also required by the observed increase in Ni and Mg contents of olivine in the mafic sill complex compared to the feeder zone (Leuthold et al., 2014).

### 6.6. The Geochemical Record of Arc Migration and Retreat in Southern Patagonia

Modern oceanic arc magmas worldwide have consistently less radiogenic Hf isotope compositions than their related back-arc, indicating ubiquitous imprinting of the subarc mantle wedge with a crustal-derived Hf component that back-arcs escape (Woodhead et al., 2012; Woodhead et al., 2001). In the same way, the retro-arc of the Patagonian continental arc would be expected to escape overprinting by the modern Hf subduction component recorded by arc magmas.

The decoupled chemical and isotopic evolution of magmatism in the retro-arc region at 49–51°S can be understood in the light of the changing geodynamic setting in southern Patagonia from 30 to 12 Ma. At ca. 30 Ma, magmatism in the Torres del Paine region was typical for a retro-arc, with low-degree melting of mantle unfluxed by recent subduction (Amarga alkaline gabbro; Fig. 11A). This low-degree mantle melting predates the ca. 25 Ma onset of Andean

uplift and intense compressive deformation in the Patagonian fold and thrust belt (Suárez et al., 2000; Thomson et al., 2001), and could possibly have occurred in response to an extensional tectonic regime in the retro-arc. An extensional setting would be consistent with the fact that convergence was slow and oblique at this time (Cande and Leslie, 1986; Somoza, 1998). From 25 to 16 Ma, a period of fast, orthogonal convergence (Cande and Leslie, 1986; Somoza, 1998) resulted in subduction erosion associated with removal of a significant quantity of forearc crust, and migration of calc-alkaline arc magmatism inboard into the (former) retro-arc region (Ramírez de Arellano et al., 2012; Thomson et al., 2001) (Fig. 11B). This migration produced a change to calc-alkaline magmatism in the Torres del Paine and Chaltén retro-arc regions from 17 to 16 Ma (Fig. 11B). The typical subduction-related chemistry and more crustal Hf isotope signatures of these intrusions record the transient addition of a subducted continental crustal component to the retro-arc mantle wedge associated with arc migration at this time. Although these intrusions range from gabbroic to granitic in composition, implying that mantle-derived melts underwent varying degrees of crustal processing to generate the different intrusions, these crustal processes did not affect their Hf isotope compositions. The change to transitional alkaline magmatism at ca. 12.6 Ma records a return to low-degree, flux-poor melting more typical of a retro-arc, after the transient inboard migration of arc magmatism had ceased (Fig. 11C). The cessation of calc-alkaline magmatism after ca. 16 Ma is also observed in the main batholith to the west: in the South Patagonian batholith, there is an abundance of 25–18 Ma plutons, but only one dated sample younger than 16 Ma (a ca. 5 Ma dacite; Hervé et al., 2007). Apart from one small ca. 14.5 Ma basaltic sub-volcanic intrusion in the retro-arc of the Chaltén region (Ramos et al., 2004), the magmas that formed the feeder zone of the TPIC at ca. 12.6 Ma were among the first melts extracted from the mantle at these latitudes after calc-alkaline magmatism vanished. The initiation of low-degree melting of the retro-arc mantle at ca. 12.6 Ma could, for example, have been caused by decompression related to the onset of a regime of extension, tectonic relaxation, and erosion around this time (Boutonnet et al., 2010; Lagabrielle et al., 2007; Lagabrielle et al., 2004) (Fig. 11C).

The first ca. 12.6 Ma low-degree melts have the same Hf isotope composition as the calc-alkaline intrusions. We propose that they were both produced by melting of mantle with a relict subduction Hf component, inherited from the last phases of fluxing of the retro-arc mantle wedge

at ca. 16 Ma (Figs. 11B, 11C). The youngest part of the TPIC, the ca. 12.45 Ma mafic sill complex, was produced by ongoing low-degree mantle melting, but has a distinctly more juvenile Hf isotope composition indistinguishable from the “background” retro-arc mantle (Fig. 8; Section 6.2). This demonstrates that by ca. 12.45 Ma, the relict subduction Hf component was exhausted from the mantle, which returned to the background retro-arc isotopic composition. We attribute this change to influx of nearby retro-arc mantle, which was not imprinted with a recent Hf subduction component, after extraction of the mantle melts that formed the oldest parts of the TPIC (Fig. 11C). In this model, the transient inboard migration of arc magmatism up to ca. 16 Ma plays a key role. During this brief period the mantle wedge previously in a retro-arc position was flushed with a subduction component (Fig. 11B). The transient nature of arc migration and the fact that, apart from this brief period, this area was rear of the arc would mean that typical subcontinental mantle, unfluxed by recent subduction, existed nearby. This proximity explains the rapid shift from a relict subduction component at ca. 12.6 Ma, to typical retro-arc mantle signatures at ca. 12.45 Ma. The close proximity of the two types of mantle is also shown by many dikes in the Torres del Paine area, which show a “hybrid” chemistry between typical calc-alkaline rocks and more alkaline varieties (Müntener et al., 2018).

The mafic sill complex has whole rock geochemistry transitional between subduction-related and alkaline magmatism, including for trace element ratios that track subduction influence, demonstrating that when it formed the relict subduction influence had been diluted but not yet completely erased for certain elements. The rapid erasure of the relict signature for Hf isotopes compared to whole rock geochemical signatures likely reflects the small quantity of Hf contributed by the subduction component, which is quickly overwhelmed with the incoming of pristine retro-arc mantle.

We have here focused our discussion of the TPIC on its mafic units, which are the most direct recorders of mantle processes. Whereas TPIC mafic units directly record input of mantle-derived magmas, the TPIC granites are interpreted as the differentiated products of the same mantle-derived melts as the older (feeder zone) mafic units, produced by fractionation from mafic cumulates in a middle crustal chamber (Leuthold et al., 2014; Leuthold et al., 2013). Although they are not directly derived from the mantle, the Hf isotope compositions of the TPIC granites are nonetheless consistent with our model, being similar to that of the feeder zone mafic units.

Ewing et al.

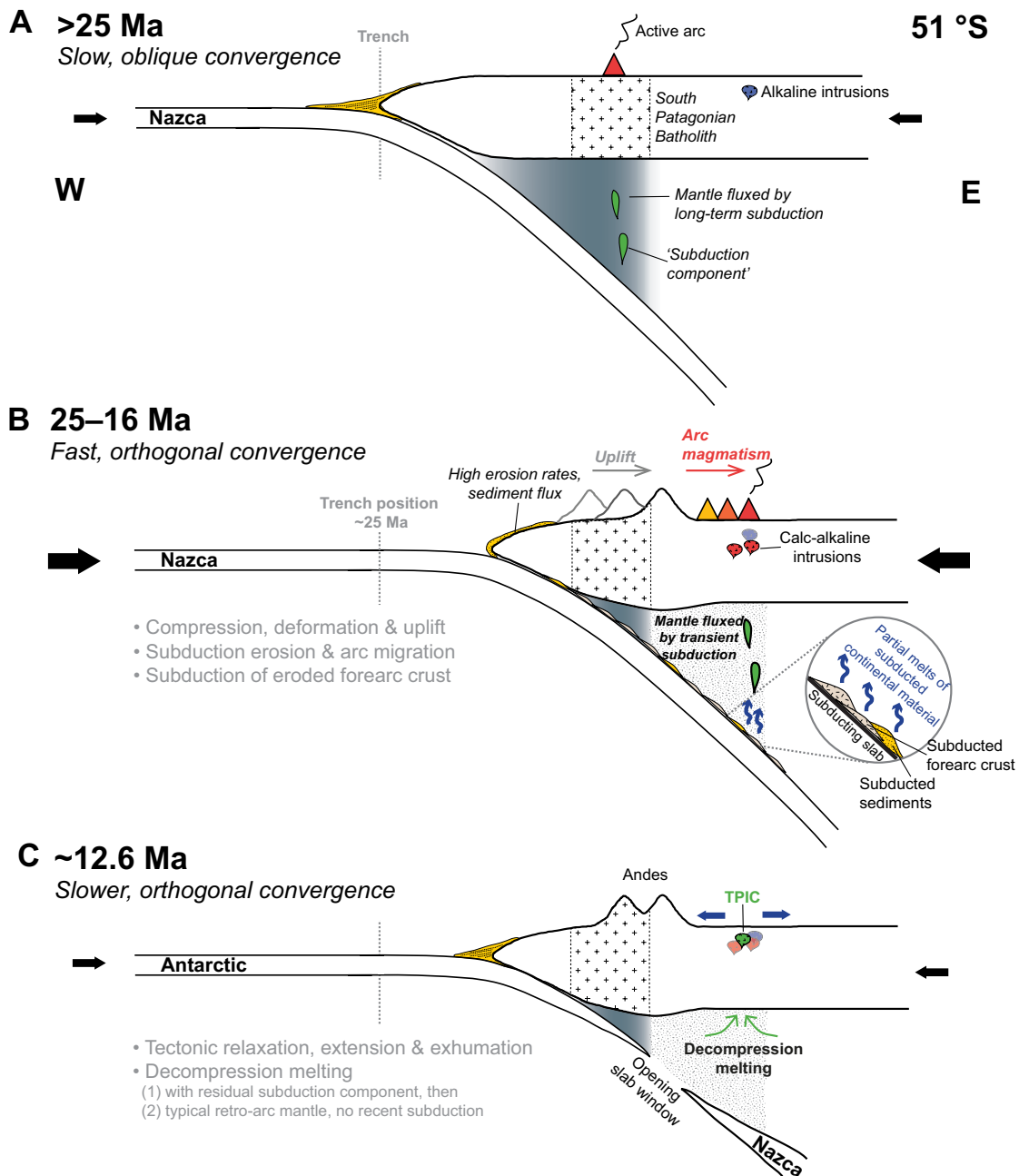


Figure 11. Schematic diagram illustrating the geodynamic evolution of the south Patagonian margin at 51°S from >25 Ma to ca. 12.6 Ma. At ca. 25 Ma, convergence changed from slow and oblique to fast and orthogonal, which initiated a period of subduction erosion of forearc crust, associated with continent-wards migration of both the trench, and calc-alkaline magmatism. This period was also characterized by compressive deformation and uplift, which migrated progressively eastwards. Increased uplift rates produced a strong orographic rain effect and intensified rainfall in the west, which led to high erosion rates and thus high sediment supply to the trench from ca. 25 Ma to 16.5 Ma (Blisniuk et al., 2005; Thomson et al., 2001). At ca. 16 Ma, convergence rates slowed (Breitsprecher and Thorkelson, 2009; Somoza, 1998) and compressive deformation ceased soon after (Fosdick et al., 2011; Lagabrielle et al., 2004; Ramírez de Arellano et al., 2012); subduction erosion is therefore likely to have terminated at this time. By ca. 12.6 Ma, when the oldest part of the Torres del Paine intrusive complex (TPIC) was emplaced, calc-alkaline magmatism was no longer active at 51°S. The Chile ridge had previously been subducted at these latitudes but the opening slab window between the Nazca and Antarctic plates was still to the west of the Torres del Paine area (Breitsprecher and Thorkelson, 2009). The TPIC was emplaced in a context of tectonic relaxation and extension, causing decompression melting of the mantle. The first mantle melts had a residual subduction Hf isotope signature related to the transient flushing of the retro-arc mantle wedge with a subduction component during the inboard migration of arc magmatism up to ca. 16 Ma. This residual subduction component was quickly exhausted and subsequent mantle melting to form the ca. 12.45 Ma TPIC mafic sill complex tapped typical retro-arc mantle uncontaminated by recent subduction.

### 6.7. Hf Isotopes as the Unique Fingerprint of Waning Subduction Influence

Trace element ratios are commonly used to trace the contribution from a subduction component to arc magmas (e.g., Plank, 2005). Although the shift in Hf isotope composition within the TPIC records the disappearance of a residual subduction Hf component, the feeder zone mafic units and mafic sill complex have similar ranges of Th/La and La/Nb, which trace the subducted sediment and slab contribution, respectively (Plank, 2005) (Fig. 9; Fig. DR13). The TPIC gabbros have clear plagioclase and hornblende textural and geochemical cumulative signatures, especially in the feeder zone (Leuthold et al., 2014; Leuthold et al., 2013). Different degrees of accumulation lead to significant scatter in major and trace element signatures between samples, that do not reflect real differences in source composition (or degree of partial melting), hampering the identification of subtle changes in trace element ratios related to the waning influence of a subduction component. A key advantage of Hf isotopes for tracing a changing subduction contribution is the ability to use an isotopic ratio, rather than elemental concentrations, to fingerprint the input of different sources. In Patagonia, subduction-fluxed mantle and ambient retro-arc mantle each have distinct, tightly clustered Hf isotope compositions ( $\epsilon_{\text{Hf}(t)}$ ) of 0 to +2.5 and  $+5.4 \pm 1.4$ , respectively). The homogenous Hf isotope compositions of these reservoirs, which are unaffected by degree of partial melting, means that even for a small change in their relative contributions, a noticeable shift in Hf isotope composition would be expected. In contrast, trace element concentrations may not change outside of the large range of absolute concentrations possible in a subduction-fluxed mantle, making these insensitive indicators of such processes.

### 6.8. The Influence of Ridge Subduction

Ridge subduction occurred at the latitudes of Torres del Paine at 13–14 Ma, and at ca. 12 Ma at the latitude of El Chaltén (Breitsprecher and Thorkelson, 2009; Cande and Leslie, 1986). Ridge subduction thus occurred after the emplacement of the ca. 16 Ma calc-alkaline intrusions, but before the ca. 12.5 Ma TPIC. We speculate that the cessation of typical subduction-related magmatism south of the present-day triple junction is at least partly a consequence of the ridge subduction, which produced a dramatic drop in convergence rate (by a factor of  $\sim 6$ ) once the Antarctic rather than the Nazca plate was subducting beneath South America (Breitsprecher and Thorkelson,

2009; Cande and Leslie, 1986). Kinematic reconstructions show that the Antarctic plate dips shallowly and reaches a maximum depth of only 45 km beneath the Austral Volcanic Zone, far too shallow to produce typical arc magmatism (Breitsprecher and Thorkelson, 2009). This dramatic drop in convergence rate for the newly subducting plate is superimposed on a general slowing of convergence rates along the Patagonian margin from ca. 16 Ma (Breitsprecher and Thorkelson, 2009; Somoza, 1998), which may also have contributed to the cessation of calc-alkaline magmatism.

The identical Hf isotope composition of magmatism before (ca. 16 Ma) and after (ca. 12.6 Ma) the ridge subduction demonstrates unequivocally that the subducting ridge was not itself involved in the petrogenesis of TPIC magmatism. If, for example, the low-degree melting that produced the TPIC was related to upwelling of sub-slab asthenosphere through an opening slab window, the observed residual subduction signature would not be recorded by the Hf isotope composition of this magmatism. That the subducted ridge was not involved in the genesis of TPIC magmatism is consistent with kinematic modeling that shows that at 12 Ma the Torres del Paine region was still inboard of the opening slab window (Breitsprecher and Thorkelson, 2009; Fig. 11), making it difficult to envisage it directly influencing magmatism in the region at this time. This conclusion is also supported by the fact that a shift from calc-alkaline magmatism at ca. 16 Ma to transitional alkaline magmatism at ca. 12 Ma is observed in the retro-arc at 47°S (Boutonnet et al., 2010; Espinoza et al., 2010), as well as at 51°S (Müntener et al., 2018; this study). The contemporaneous occurrence of low-degree melting in southernmost Patagonia and at the latitude of the present-day triple junction, while ridge subduction occurred some 14 m.y. apart at these latitudes (Breitsprecher and Thorkelson, 2009), strongly argues against the subducted ridge itself being directly involved in the petrogenesis of these magmas. The main role of the ridge subduction in governing magmatism in the region is thus to induce the shift from calc-alkaline magmatism to low-degree mantle melting, as a result of the changed convergence rate of the new subducting plate.

## CONCLUSIONS

Hf isotopic variability is preserved in southern Patagonian (49–51°S) magmatic units on different time scales. An extremely rapid change in only a few thousand to tens of thousands of years ( $20 \pm 10$  k.y.) is observed within the exceptionally well-exposed Torres del Paine

sheeted intrusion, whereas a regional change occurred during an important period of arc migration between 30 and 12 Ma. We have shown that the observed changes in Hf isotope compositions directly reflect changes in the mantle source tapped by these magmatic units. We infer that the different Hf isotopic compositions are related to the shifting influence of the subducting plate: the more alkaline-rich intrusions tap a “background subcontinental mantle,” whereas calc-alkaline plutons tap a mantle that is affected by subducted continental crustal components. The regional Hf isotopic evolution of intrusions in southern Patagonia thus tracks the transient migration of subduction-related magmatism into the south Patagonian retro-arc until ca. 16 Ma, and the progressive return to low-degree melting after fluxing of the retro-arc mantle ceased. The “background sub-continental mantle,” as characterized by a ca. 30 Ma alkaline gabbro, is shown to have an inherently enriched Hf isotope composition. Numerous ca. 17–12.5 Ma plutons in the Torres del Paine and El Chaltén regions have remarkably consistent, slightly more enriched  $\epsilon_{\text{Hf}(t)}$  over large temporal and spatial scales of  $>4$  m.y. and  $\sim 200$  km. These tightly clustered Hf isotope compositions record input of subducted continental components into the retro-arc mantle, associated with the continent-wards migration of arc magmatism up to ca. 16 Ma. A rapid return to low degree, relatively unfluxed mantle melting is recorded in the retro-arc Torres del Paine sheeted intrusion. The oldest (ca. 12.6 Ma) part of the TPIC was produced by melting of mantle with a relict subduction component with identical  $\epsilon_{\text{Hf}(t)}$  to the previous calc-alkaline magmatism. An abrupt shift to distinctly more juvenile Hf isotope signatures in the youngest (ca. 12.45 Ma) part of the TPIC occurred within  $20 \pm 10$  k.y. and records melting of typical “background” retro-arc mantle, after the relict subduction component was exhausted. This change in isotopic composition demonstrates that within a single intrusive complex built up over  $<200$  k.y., different magma batches can tap geochemically different mantle reservoirs. Furthermore, our results show that migration of arc magmatism into the retro-arc region for only a few million years is sufficient to significantly modify the composition of the retro-arc mantle wedge, imprinting it with a distinct subduction signature. We propose that the Hf isotope composition of zircon is the most sensitive tracer of the waning influence of subduction in the Patagonian retro-arc. The finding that a shallow crustal pluton taps different mantle sources on 10 k.y. timescales has profound implications for our understanding of the process of melt transport in transcrustal magmatic mush columns.

## ACKNOWLEDGMENTS

We thank Massimo Chiaradia and François-Xavier D'Abzac for their support and scientific discussions relating to the measurement of Hf isotopes on the Neptune Plus, Pierre Vonlanthen for assistance with the scanning electron microscope, and Benita Putlitz for scientific discussions. We are grateful to Christopher Fisher and John Hanchar for kindly supplying us with their synthetic zircon standards. We thank the authorities of the Torres del Paine National Park in Chile's Patagonia region, and Chile's Corporación Nacional Forestal (CONAF) for permission and support to work in the Torres del Paine region. We are grateful to Mélina Manzini, Thibaud Roux, Luc Allemann, and Pierre Pellaud for sharing their samples and information on them. We thank Rosemary Jones and Roland Maas for their constructive reviews that helped improve the manuscript, and Jocelyn McPhie and Aaron Cavosie for detailed and efficient editorial handling and review. We gratefully acknowledge access to the MC-ICPMS facility in Geneva, Switzerland, which was established thanks to the financial support of the Swiss National Science Foundation and the Universities of Geneva and Lausanne. This work was financially supported by the Swiss National Science Foundation projects 200021-162666 (to O.M.) and 200020-139178 (to O.M. and U.S.), and 200020-120120 and 200020-140974 (to L.P.B.), the Herbetta Foundation, and generous funding from the University of Lausanne. J.L. acknowledges support from a Swiss National Science Foundation Ambizione grant.

## REFERENCES CITED

- Amelin, Y., and Davis, W.J., 2005, Geochemical test for branching decay of Lu-176: *Geochimica et Cosmochimica Acta*, v. 69, no. 2, p. 465–473, <https://doi.org/10.1016/j.gca.2004.04.028>.
- Assumpção, M., Feng, M., Tassara, A., and Julià, J., 2013, Models of crustal thickness for South America from seismic refraction, receiver functions and surface wave tomography: *Tectonophysics*, v. 609, p. 82–96, <https://doi.org/10.1016/j.tecto.2012.11.014>.
- Augustsson, C., Münker, C., Bahlburg, H., and Fanning, C.M., 2006, Provenance of late Palaeozoic metasediments of the SW South American Gondwana margin: A combined U–Pb and Hf-isotope study of single detrital zircons: *Journal of the Geological Society*, v. 163, no. 6, p. 983–995, <https://doi.org/10.1144/0016-76492005-149>.
- Barboni, M., Annen, C., and Schoene, B., 2015, Evaluating the construction and evolution of upper crustal magma reservoirs with coupled U/Pb zircon geochronology and thermal modeling: A case study from the Mt. Capanne pluton (Elba, Italy): *Earth and Planetary Science Letters*, v. 432, p. 436–448, <https://doi.org/10.1016/j.epsl.2015.09.043>.
- Blisniuk, P.M., Stern, L.A., Chamberlain, C.P., Idleman, B., and Zeitler, P.K., 2005, Climatic and ecologic changes during Miocene surface uplift in the Southern Patagonian Andes: *Earth and Planetary Science Letters*, v. 230, no. 1–2, p. 125–142, <https://doi.org/10.1016/j.epsl.2004.11.015>.
- Boutonnet, E., Arnaud, N., Guivel, C., Lagabrielle, Y., Scablirino, B., and Espinoza, F., 2010, Subduction of the South Chile active spreading ridge: A 17 Ma to 3 Ma magmatic record in central Patagonia (western edge of Meseta del Lago Buenos Aires, Argentina): *Journal of Volcanology and Geothermal Research*, v. 189, no. 3–4, p. 319–339, <https://doi.org/10.1016/j.jvolgeores.2009.11.022>.
- Bouvier, A., Vervoort, J.D., and Patchett, P.J., 2008, The Lu–Hf and Sm–Nd isotopic composition of CHUR: Constraints from unequilibrated chondrites and implications for the bulk composition of terrestrial planets: *Earth and Planetary Science Letters*, v. 273, no. 1–2, p. 48–57, <https://doi.org/10.1016/j.epsl.2008.06.010>.
- Breitsprecher, K., and Thorkelson, D.J., 2009, Neogene kinematic history of Nazca–Antarctic–Phoenix slab windows beneath Patagonia and the Antarctic Peninsula: *Tectonophysics*, v. 464, no. 1–4, p. 10–20, <https://doi.org/10.1016/j.tecto.2008.02.013>.
- Broderick, C., Wotzlaw, J.F., Frick, D.A., Gerdes, A., Ulianov, A., Günther, D., and Schaltegger, U., 2015, Linking the thermal evolution and emplacement history of an upper-crustal pluton to its lower-crustal roots using zircon geochronology and geochemistry (southern Adamello batholith, N. Italy): *Contributions to Mineralogy and Petrology*, v. 170, no. 3, p. 28, <https://doi.org/10.1007/s00410-015-1184-x> (An erratum to this paper can be found at <http://dx.doi.org/10.1007/s00410-016-1240-1>).
- Cande, S.C., and Leslie, R.B., 1986, Late Cenozoic tectonics of the Southern Chile Trench: *Journal of Geophysical Research, Solid Earth*, v. 91, no. B1, p. 471–496, <https://doi.org/10.1029/JB091iB01p00471>.
- Chu, N.C., Taylor, R.N., Chavagnac, V., Nesbitt, R.W., Boella, R.M., Milton, J.A., German, C.R., Bayon, G., and Burton, K., 2002, Hf isotope ratio analysis using multi-collector inductively coupled plasma mass spectrometry: An evaluation of isobaric interference corrections: *Journal of Analytical Atomic Spectrometry*, v. 17, no. 12, p. 1567–1574, <https://doi.org/10.1039/b206707b>.
- Claiborne, L.L., Miller, C.F., Flanagan, D.M., Clyne, M.A., and Wooden, J.L., 2010, Zircon reveals protracted magma storage and recycling beneath Mount St. Helens: *Geology*, v. 38, no. 11, p. 1011–1014, <https://doi.org/10.1130/G31285.1>.
- Coleman, D.S., Gray, W., and Glazner, A.F., 2004, Rethinking the emplacement and evolution of zoned plutons: Geochronologic evidence for incremental assembly of the Tuolumne Intrusive Suite, California: *Geology*, v. 32, no. 5, p. 433–436, <https://doi.org/10.1130/G20220.1>.
- D'Abzac, F.-X., Davies, J.H.F.L., Wotzlaw, J.-F., and Schaltegger, U., 2016, Hf isotope analysis of small zircon and baddeleyite grains by conventional multi collector-inductively coupled plasma-mass spectrometry: *Chemical Geology*, v. 433, p. 12–23, <https://doi.org/10.1016/j.chemgeo.2016.03.025>.
- Dhuime, B., Hawkesworth, C.J., Cawood, P.A., and Storey, C.D., 2012, A change in the geodynamics of continental growth 3 billion years ago: *Science*, v. 335, no. 6074, p. 1334–1336, <https://doi.org/10.1126/science.1216066>.
- Durrant, S.F., 1994, Feasibility of improvement in analytical performance in laser-ablation inductively-coupled plasma-mass spectrometry (LA-ICP-MS) by addition of nitrogen to the argon plasma: *Fresenius' Journal of Analytical Chemistry*, v. 349, no. 10–11, p. 768–771, <https://doi.org/10.1007/BF00325655>.
- Eggins, S.M., Kinsley, L.P.J., and Shelley, J.M.G., 1998, Deposition and element fractionation processes during atmospheric pressure laser sampling for analysis by ICP-MS: *Applied Surface Science*, v. 129, p. 278–286, [https://doi.org/10.1016/S0169-4332\(97\)00643-0](https://doi.org/10.1016/S0169-4332(97)00643-0).
- Espinoza, F., Morata, D., Pelleter, E., Maury, R.C., Suárez, M., Lagabrielle, Y., Polvé, M., Bellon, H., Cotten, J., and De la Cruz, R., 2005, Petrogenesis of the Eocene and Mio–Pliocene alkaline basaltic magmatism in Meseta Chile Chico, southern Patagonia, Chile: Evidence for the participation of two slab windows: *Lithos*, v. 82, no. 3, p. 315–343, <https://doi.org/10.1016/j.lithos.2004.09.024>.
- Espinoza, F., Morata, D., Polve, M., Lagabrielle, Y., Maury, R., de la Rupelle, A., Guivel, C., Cotten, J., Bellon, H., and Suarez, M., 2010, Middle Miocene calc-alkaline volcanism in Central Patagonia (47°S): Petrogenesis and implications for slab dynamics: *Andean Geology*, v. 37, no. 2, p. 300–328, <https://doi.org/10.5027/andgeoV37n2-a03>.
- Ewing, T.A., Rubatto, D., Eggins, S.M., and Hermann, J., 2011, In situ measurement of hafnium isotopes in rutile by LA-MC-ICPMS: Protocol and applications: *Chemical Geology*, v. 281, no. 1–2, p. 72–82, <https://doi.org/10.1016/j.chemgeo.2010.11.029>.
- Fisher, C.M., Hanchar, J.M., Samson, S.D., Dhuime, B., Blichert-Toft, J., Vervoort, J.D., and Lam, R., 2011, Synthetic zircon doped with hafnium and rare earth elements: A reference material for in situ hafnium isotope analysis: *Chemical Geology*, v. 286, no. 1–2, p. 32–47, <https://doi.org/10.1016/j.chemgeo.2011.04.013>.
- Fisher, C.M., Vervoort, J.D., and Hanchar, J.M., 2014, Guidelines for reporting zircon Hf isotopic data by LA-MC-ICPMS and potential pitfalls in the interpretation of these data: *Chemical Geology*, v. 363, p. 125–133, <https://doi.org/10.1016/j.chemgeo.2013.10.019>.
- Forsythe, R., and Prior, D., 1992, Cenozoic continental geology of South America and its relations to the evolution of the Chile triple junction, in Behrmann, J.H., Lewis, S.D., Musgrave, R.J., eds., *Proceedings of the Ocean Drilling Program, Initial Reports*, 141: College Station, Texas, USA, Ocean Drilling Program, p. 23–31, <https://doi.org/10.2973/odp.proc.ir.141.103.1992>.
- Fosdick, J.C., Romans, B.W., Fildani, A., Bernhardt, A., Calderón, M., and Graham, S.A., 2011, Kinematic evolution of the Patagonian retroarc fold-and-thrust belt and Magallanes foreland basin, Chile and Argentina, 51°30'S: *Geological Society of America Bulletin*, v. 123, no. 9–10, p. 1679–1698, <https://doi.org/10.1130/B30242.1>.
- Fosdick, J.C., Grove, M., Hourigan, J.K., and Calderón, M., 2013, Retroarc deformation and exhumation near the end of the Andes, southern Patagonia: *Earth and Planetary Science Letters*, v. 361, p. 504–517, <https://doi.org/10.1016/j.epsl.2012.12.007>.
- Ghiglione, M.C., Ramos, V.A., Cuitiño, J., and Barberón, V., 2016, Growth of the Southern Patagonian Andes (46–53°S) and Their Relation to Subduction Processes, in Folguera, A., Naipauer, M., Sagripanti, L., Ghiglione, C.M., Orts, L.D., and Giambiagi, L., eds., *Growth of the Southern Andes*: Cham, Switzerland, Springer International Publishing, p. 201–240, <https://doi.org/10.1007/978-3-319-23060-3>.
- Glazner, A.F., Bartley, J.M., Coleman, D.S., Gray, W., and Taylor, R.Z., 2004, Are plutons assembled over millions of years by amalgamation from small magma chambers?: *GSA Today*, v. 14, no. 4–5, p. 4–12, [https://doi.org/10.1130/1052-5173\(2004\)014<0004:APAOM>2.0.CO;2](https://doi.org/10.1130/1052-5173(2004)014<0004:APAOM>2.0.CO;2).
- Gorring, M.L., Kay, S.M., Zeitler, P.K., Ramos, V.A., Rubiolo, D., Fernandez, M.I., and Panza, J.L., 1997, Neogene Patagonian plateau lavas: Continental magmas associated with ridge collision at the Chile Triple Junction: *Tectonics*, v. 16, no. 1, p. 1–17, <https://doi.org/10.1029/96TC03368>.
- Guivel, C., Morata, D., Pelleter, E., Espinoza, F., Maury, R.C., Lagabrielle, Y., Polvé, M., Bellon, H., Cotten, J., Benoit, M., Suárez, M., and de la Cruz, R., 2006, Miocene to Late Quaternary Patagonian basalts (46–47°S): Geochronometric and geochemical evidence for slab tearing due to active spreading ridge subduction: *Journal of Volcanology and Geothermal Research*, v. 149, no. 3–4, p. 346–370, <https://doi.org/10.1016/j.jvolgeores.2005.09.002>.
- Hervé, F., Fanning, C.M., and Pankhurst, R.J., 2003, Detrital zircon age patterns and provenance of the metamorphic complexes of southern Chile: *Journal of South American Earth Sciences*, v. 16, no. 1, p. 107–123, [https://doi.org/10.1016/S0895-9811\(03\)00022-1](https://doi.org/10.1016/S0895-9811(03)00022-1).
- Hervé, F., Pankhurst, R.J., Fanning, C.M., Calderón, M., and Yaxley, G.M., 2007, The South Patagonian batholith: 150 my of granite magmatism on a plate margin: *Lithos*, v. 97, no. 3–4, p. 373–394, <https://doi.org/10.1016/j.lithos.2007.01.007>.
- Hoskin, P.W.O., and Black, L.P., 2000, Metamorphic zircon formation by solid-state recrystallization of protolith igneous zircon: *Journal of Metamorphic Geology*, v. 18, no. 4, p. 423–439, <https://doi.org/10.1046/j.1525-1314.2000.00266.x>.
- Hoskin, P.W.O., and Schaltegger, U., 2003, The composition of zircon and igneous and metamorphic petrogenesis, in Hanchar, J.M., and Hoskin, P.W.O., eds., *Zircon: Reviews in Mineralogy and Geochemistry*: Washington, DC, Mineralogical Society of America, v. 53, p. 27–62, <https://doi.org/10.2113/0530027>.
- Iizuka, T., and Hirata, T., 2005, Improvements of precision and accuracy in in situ Hf isotope microanalysis of zircon using the laser ablation-MC-ICPMS technique:

## Rapidly changing mantle sources in the south Patagonian retro-arc

- Chemical Geology, v. 220, no. 1-2, p. 121–137, <https://doi.org/10.1016/j.chemgeo.2005.03.010>.
- Irvine, T.N., and Baragar, W.R.A., 1971, A guide to the chemical classification of the common volcanic rocks: *Canadian Journal of Earth Sciences*, v. 8, no. 5, p. 523–548, <https://doi.org/10.1139/e71-055>.
- Jones, R.E., Kirstein, L.A., Kasemann, S.A., Dhuime, B., Elliott, T., Litvak, V.D., Alonso, R., and Hinton, R., 2015, Geodynamic controls on the contamination of Cenozoic arc magmas in the southern Central Andes: Insights from the O and Hf isotopic composition of zircon: *Geochimica et Cosmochimica Acta*, v. 164, p. 386–402, <https://doi.org/10.1016/j.gca.2015.05.007>.
- Kay, S.M., Gorrung, M., and Ramos, V.A., 2004, Magmatic sources, setting and causes of Eocene to Recent Patagonian plateau magmatism (36°S to 52°S latitude): *Revista de la Asociación Geológica Argentina*, v. 59, no. 4, p. 556–568.
- Kemp, A.I.S., Hawkesworth, C.J., Foster, G.L., Paterson, B.A., Woodhead, J.D., Hergt, J.M., Gray, C.M., and Whitehouse, M.J., 2007, Magmatic and crustal differentiation history of granitic rocks from Hf-O isotopes in zircon: *Science*, v. 315, no. 5814, p. 980–983, <https://doi.org/10.1126/science.1136154>.
- Kemp, A.I.S., Foster, G.L., Scherstin, A., Whitehouse, M.J., Darling, J., and Storey, C., 2009, Concurrent Pb–Hf isotope analysis of zircon by laser ablation multi-collector ICP-MS, with implications for the crustal evolution of Greenland and the Himalayas: *Chemical Geology*, v. 261, no. 3-4, p. 244–260, <https://doi.org/10.1016/j.chemgeo.2008.06.019>.
- Kinny, P.D., Compston, W., and Williams, I.S., 1991, A reconnaissance ion-probe study of hafnium isotopes in zircons: *Geochimica et Cosmochimica Acta*, v. 55, no. 3, p. 849–859, [https://doi.org/10.1016/0016-7037\(91\)90346-7](https://doi.org/10.1016/0016-7037(91)90346-7).
- Lagabriele, Y., Suárez, M., Rossello, E.A., Hérial, G., Martinot, J., Régnier, M., and de la Cruz, R., 2004, Neogene to Quaternary tectonic evolution of the Patagonian Andes at the latitude of the Chile Triple Junction: *Tectonophysics*, v. 385, no. 1-4, p. 211–241, <https://doi.org/10.1016/j.tecto.2004.04.023>.
- Lagabriele, Y., Suárez, M., Malavieille, J., Morata, D., Espinoza, F., Maury, R.C., Scalabrino, B., Barbero, L., de la Cruz, R., Rossello, E., and Bellon, H., 2007, Pliocene extensional tectonics in the Eastern Central Patagonian Cordillera: Geochronological constraints and new field evidence: *Terra Nova*, v. 19, no. 6, p. 413–424, <https://doi.org/10.1111/j.1365-3121.2007.00766.x>.
- Lawrence, J.F., and Wiens, D.A., 2004, Combined receiver-function and surface wave phase-velocity inversion using a niching genetic algorithm: Application to Patagonia: *Bulletin of the Seismological Society of America*, v. 94, no. 3, p. 977–987, <https://doi.org/10.1785/0120030172>.
- Leuthold, J., Müntener, O., Baumgartner, L.P., Putlitz, B., Ovtcharova, M., and Schaltegger, U., 2012, Time resolved construction of a bimodal laccolith (Torres del Paine, Patagonia): *Earth and Planetary Science Letters*, v. 325, p. 85–92, <https://doi.org/10.1016/j.epsl.2012.01.032>.
- Leuthold, J., Müntener, O., Baumgartner, L.P., Putlitz, B., and Chiaradia, M., 2013, A detailed geochemical study of a shallow arc-related laccolith: the Torres del Paine Mafic Complex (Patagonia): *Journal of Petrology*, v. 54, no. 2, p. 273–303, <https://doi.org/10.1093/petrology/egs069>.
- Leuthold, J., Müntener, O., Baumgartner, L.P., and Putlitz, B., 2014, Petrological Constraints on the Recycling of Mafic Crystal Mushes and Intrusion of Braided Sills in the Torres del Paine mafic complex (Patagonia): *Journal of Petrology*, v. 55, no. 5, p. 917–949, <https://doi.org/10.1093/petrology/egu011>.
- Manzini, M., 2012, Géochimie et géochronologie des roches ignées du SE du parc national de Torres del Paine, Chili [unpublished M.S. thesis]: University of Lausanne, Switzerland, 116 p.
- McDonough, W.F., and Sun, S.S., 1995, The composition of the Earth: *Chemical Geology*, v. 120, no. 3-4, p. 223–253, [https://doi.org/10.1016/0009-2541\(94\)00140-4](https://doi.org/10.1016/0009-2541(94)00140-4).
- Michael, P.J., 1984, Chemical differentiation of the Cordillera Paine granite (southern Chile) by in situ fractional crystallization: *Contributions to Mineralogy and Petrology*, v. 87, no. 2, p. 179–195, <https://doi.org/10.1007/BF00376223>.
- Michael, P.J., 1991, Intrusion of basaltic magma into a crystallizing granitic magma chamber: The Cordillera del Paine pluton in southern Chile: *Contributions to Mineralogy and Petrology*, v. 108, no. 4, p. 396–418, <https://doi.org/10.1007/BF00303446>.
- Michel, J., Baumgartner, L., Putlitz, B., Schaltegger, U., and Ovtcharova, M., 2008, Incremental growth of the Patagonian Torres del Paine laccolith over 90 k.y.: *Geology*, v. 36, no. 6, p. 459–462, <https://doi.org/10.1130/G24546A.1>.
- Morel, M.L.A., Nebel, O., Nebel-Jacobsen, Y.J., Miller, J.S., and Vroon, P.Z., 2008, Hafnium isotope characterization of the GJ-1 zircon reference material by solution and laser-ablation MC-ICP-MS: *Chemical Geology*, v. 255, no. 1-2, p. 231–235, <https://doi.org/10.1016/j.chemgeo.2008.06.040>.
- Müntener, O., Ewing, T.A., Baumgartner, L.P., Manzini, M., Roux, T., Pellaud, P., and Allemann, L., 2018, Source and fractionation controls on subduction-related plutons and dike swarms in southern Patagonia (Torres del Paine area) and the low Nb/Ta of upper crustal igneous rocks: *Contributions to Mineralogy and Petrology*, v. 173, no. 5, p. 38, <https://doi.org/10.1007/s00410-018-1467-0>.
- Nebel, O., Vroon, P.Z., van Westrenen, W., Izuka, T., and Davies, G.R., 2011, The effect of sediment recycling in subduction zones on the Hf isotope character of new arc crust, Banda arc, Indonesia: *Earth and Planetary Science Letters*, v. 303, p. 240–250, <https://doi.org/10.1016/j.epsl.2010.12.053>.
- Nowell, G.M., Kempton, P.D., Noble, S.R., Fitton, J.G., Saunders, A.D., Mahoney, J.J., and Taylor, R.N., 1998, High precision Hf isotope measurements of MORB and OIB by thermal ionisation mass spectrometry: Insights into the depleted mantle: *Chemical Geology*, v. 149, no. 3-4, p. 211–233, [https://doi.org/10.1016/S0009-2541\(98\)00036-9](https://doi.org/10.1016/S0009-2541(98)00036-9).
- Patchett, P.J., and Tatsumoto, M., 1981, A routine high-precision method for Lu-Hf isotope geochemistry and chronology: *Contributions to Mineralogy and Petrology*, v. 75, no. 3, p. 263–267, <https://doi.org/10.1007/BF01166766>.
- Payne, J.L., Pearson, N.J., Grant, K.J., and Halverson, G.P., 2013, Reassessment of relative oxide formation rates and molecular interferences on in situ lutetium-hafnium analysis with laser ablation MC-ICP-MS: *Journal of Analytical Atomic Spectrometry*, v. 28, no. 7, p. 1068–1079, <https://doi.org/10.1039/c3ja50090j>.
- Plank, T., 2005, Constraints from thorium/lanthanum on sediment recycling at subduction zones and the evolution of the continents: *Journal of Petrology*, v. 46, no. 5, p. 921–944, <https://doi.org/10.1093/petrology/egi005>.
- Ramírez de Arellano, C., Putlitz, B., Müntener, O., and Ovtcharova, M., 2012, High precision U/Pb zircon dating of the Chaltén Plutonic Complex (Cerro Fitz Roy, Patagonia) and its relationship to arc migration in the southernmost Andes: *Tectonics*, v. 31, no. 4, TC4009, <https://doi.org/10.1029/2011TC003048>.
- Ramos, V.A., 2010, The Grenville-age basement of the Andes: *Journal of South American Earth Sciences*, v. 29, no. 1, p. 77–91, <https://doi.org/10.1016/j.jsames.2009.09.004>.
- Ramos, V.A., and Folguera, A., 2011, Payenia volcanic province in the Southern Andes: An appraisal of an exceptional Quaternary tectonic setting: *Journal of Volcanology and Geothermal Research*, v. 201, no. 1-4, p. 53–64, <https://doi.org/10.1016/j.jvolgeores.2010.09.008>.
- Ramos, V.A., and Kay, S.M., 1992, Andean geodynamics Southern Patagonian plateau basalts and deformation: Backarc testimony of ridge collisions: *Tectonophysics*, v. 205, no. 1, p. 261–282, [https://doi.org/10.1016/0040-1951\(92\)90430-E](https://doi.org/10.1016/0040-1951(92)90430-E).
- Ramos, V.A., Kay, S., and Singer, B.S., 2004, Las adakitas de la Cordillera Patagónica: Nuevas evidencias geocímicas y geocronológicas: *Revista de la Asociación Geológica Argentina*, v. 59, no. 4, p. 693–706.
- Ranero, C.R., and von Huene, R., 2000, Subduction erosion along the Middle America convergent margin: *Nature*, v. 404, no. 6779, p. 748–752, <https://doi.org/10.1038/35008046>.
- Rivalenti, G., Mazzucchelli, M., Laurora, A., Ciuffi, S.I.A., Zanetti, A., Vannucci, R., and Cingolani, C.A., 2004, The backarc mantle lithosphere in Patagonia, South America: *Journal of South American Earth Sciences*, v. 17, no. 2, p. 121–152, <https://doi.org/10.1016/j.jsames.2004.05.009>.
- Robertson Maurice, S.D., Wiens, D.A., Koper, K.D., and Vera, E., 2003, Crustal and upper mantle structure of southernmost South America inferred from regional waveform inversion: *Journal of Geophysical Research*, Solid Earth, v. 108, no. B1, <https://doi.org/10.1029/2002JB001828>.
- Rollinson, H.R., 1993, *Using Geochemical Data: Evaluation, Presentation, Interpretation*: Harlow, UK: New York, USA, Longman Scientific and Technical, 352 p.
- Russell, W.A., Papanastassiou, D.A., and Tombrello, T.A., 1978, Ca isotope fractionation on the Earth and other solar system materials: *Geochimica et Cosmochimica Acta*, v. 42, no. 8, p. 1075–1090, [https://doi.org/10.1016/0016-7037\(78\)90105-9](https://doi.org/10.1016/0016-7037(78)90105-9).
- Schaltegger, U., Brack, P., Ovtcharova, M., Peytcheva, I., Schoene, B., Stracke, A., Marocchi, M., and Bargossi, G.M., 2009, Zircon and titanite recording 1.5 million years of magma accretion, crystallization and initial cooling in a composite pluton (southern Adamello batholith, northern Italy): *Earth and Planetary Science Letters*, v. 286, no. 1-2, p. 208–218, <https://doi.org/10.1016/j.epsl.2009.06.028>.
- Schmitt, A.K., Danišik, M., Evans, N.J., Siebel, W., Kiemle, E., Aydin, F., and Harvey, J.C., 2011, Acigöl rhyolite field, Central Anatolia (part 1): High-resolution dating of eruption episodes and zircon growth rates: *Contributions to Mineralogy and Petrology*, v. 162, no. 6, p. 1215–1231, <https://doi.org/10.1007/s00410-011-0648-x>.
- Schoene, B., Schaltegger, U., Brack, P., Latkoczy, C., Stracke, A., and Günther, D., 2012, Rates of magma differentiation and emplacement in a ballooning pluton recorded by U–Pb TIMS-TEA, Adamello batholith, Italy: *Earth and Planetary Science Letters*, v. 355–356, p. 162–173, <https://doi.org/10.1016/j.epsl.2012.08.019>.
- Segal, I., Halicz, L., and Platzner, I.T., 2003, Accurate isotope ratio measurements of ytterbium by multiple collection inductively coupled plasma mass spectrometry applying erbium and hafnium in an improved double external normalization procedure: *Journal of Analytical Atomic Spectrometry*, v. 18, no. 10, p. 1217–1223, <https://doi.org/10.1039/b307016f>.
- Sláma, J., Košler, J., Condon, D.J., Crowley, J.L., Gerdes, A., Hanchar, J.M., Horstwood, M.S.A., Morris, G.A., Nasdala, L., Norberg, N., Schaltegger, U., Schoene, B., Tubrett, M.N., and Whitehouse, M.J., 2008, Plešovice zircon: A new natural reference material for U–Pb and Hf isotopic microanalysis: *Chemical Geology*, v. 249, no. 1-2, p. 1–35, <https://doi.org/10.1016/j.chemgeo.2007.11.005>.
- Söderlund, U., Patchett, J.P., Vervoort, J.D., and Isachsen, C.E., 2004, The <sup>176</sup>Lu decay constant determined by Lu–Hf and U–Pb isotope systematics of Precambrian mafic intrusions: *Earth and Planetary Science Letters*, v. 219, no. 3-4, p. 311–324, [https://doi.org/10.1016/S0012-821X\(04\)00012-3](https://doi.org/10.1016/S0012-821X(04)00012-3).
- Somoza, R., 1998, Updated Nazca (Farallon)–South America relative motions during the last 40 My: Implications for mountain building in the central Andean region: *Journal of South American Earth Sciences*, v. 11, no. 3, p. 211–215, [https://doi.org/10.1016/S0895-9811\(98\)00012-1](https://doi.org/10.1016/S0895-9811(98)00012-1).
- Stern, C.R., and Kilian, R., 1996, Role of the subducted slab, mantle wedge and continental crust in the generation of adakites from the Andean Austral Volcanic Zone: *Contributions to Mineralogy and Petrology*, v. 123, no. 3, p. 263–281, <https://doi.org/10.1007/s004100050155>.
- Straub, S.M., Gómez-Tuena, A., Bindeman, I.N., Bolge, L.L., Brandl, P.A., Espinasa-Perena, R., Solari, L., Stuart, F.M., Vannucchi, P., and Zellmer, G.F., 2015, Crustal recycling by subduction erosion in the central Mexican Volcanic Belt: *Geochimica et Cosmochimica Acta*, v. 166, p. 29–52, <https://doi.org/10.1016/j.gca>

- .2015.06.001. (A corrigendum to this paper can be found at <http://dx.doi.org/10.1016/j.gca.2015.09.028>.)
- Suárez, M., De La Cruz, R., and Bell, C.M., 2000, Timing and origin of deformation along the Patagonian fold and thrust belt: *Geological Magazine*, v. 137, no. 4, p. 345–353, <https://doi.org/10.1017/S0016756800004192>.
- Thirlwall, M.F., and Anczkiewicz, R., 2004, Multidynamic isotope ratio analysis using MC-ICP-MS and the causes of secular drift in Hf, Nd and Pb isotope ratios: *International Journal of Mass Spectrometry*, v. 235, no. 1, p. 59–81, <https://doi.org/10.1016/j.ijms.2004.04.002>.
- Thompson, A.B., Matile, L., and Ulmer, P., 2002, Some thermal constraints on crustal assimilation during fractionation of hydrous, mantle-derived magmas with examples from central alpine batholiths: *Journal of Petrology*, v. 43, no. 3, p. 403–422, <https://doi.org/10.1093/ptrology/43.3.403>.
- Thomson, S.N., Hervé, F., and Stöckhert, B., 2001, Mesozoic-Cenozoic denudation history of the Patagonian Andes (southern Chile) and its correlation to different subduction processes: *Tectonics*, v. 20, no. 5, p. 693–711, <https://doi.org/10.1029/2001TC900013>.
- Thomson, S.N., Brandon, M.T., Tomkin, J.H., Reiners, P.W., Vasquez, C., and Wilson, N.J., 2010, Glaciation as a destructive and constructive control on mountain building: *Nature*, v. 467, no. 7313, p. 313–317, <https://doi.org/10.1038/nature09365>.
- Vervoort, J.D., Patchett, P.J., Blichert-Toft, J., and Albarede, F., 1999, Relationships between Lu-Hf and Sm-Nd isotopic systems in the global sedimentary system: *Earth and Planetary Science Letters*, v. 168, no. 1–2, p. 79–99, [https://doi.org/10.1016/S0012-821X\(99\)00047-3](https://doi.org/10.1016/S0012-821X(99)00047-3).
- Vervoort, J.D., Patchett, P.J., Soderlund, U., and Baker, M., 2004, Isotopic composition of Yb and the determination of Lu concentrations and Lu/Hf ratios by isotope dilution using MC-ICPMS: *Geochemistry, Geophysics, Geosystems*, v. 5, Q11002, <https://doi.org/10.1029/2004GC000721>.
- Wilson, T., 1991, Transition from back-arc to foreland basin development in the southernmost Andes: Stratigraphic record from the Ultima Esperanza District, Chile: *Geological Society of America Bulletin*, v. 103, no. 1, p. 98–111, [https://doi.org/10.1130/0016-7606\(1991\)103<0098:TFBATF>2.3.CO;2](https://doi.org/10.1130/0016-7606(1991)103<0098:TFBATF>2.3.CO;2).
- Woodhead, J.D., and Hergt, J.M., 2005, A preliminary appraisal of seven natural zircon reference materials for in situ Hf isotope determination: *Geostandards and Geoanalytical Research*, v. 29, no. 2, p. 183–195, <https://doi.org/10.1111/j.1751-908X.2005.tb00891.x>.
- Woodhead, J.D., Hergt, J.M., Davidson, J.P., and Eggins, S.M., 2001, Hafnium isotope evidence for 'conservative' element mobility during subduction zone processes: *Earth and Planetary Science Letters*, v. 192, no. 3, p. 331–346, [https://doi.org/10.1016/S0012-821X\(01\)00453-8](https://doi.org/10.1016/S0012-821X(01)00453-8).
- Woodhead, J., Hergt, J., Shelley, M., Eggins, S., and Kemp, R., 2004, Zircon Hf-isotope analysis with an excimer laser, depth profiling, ablation of complex geometries, and concomitant age estimation: *Chemical Geology*, v. 209, no. 1–2, p. 121–135, <https://doi.org/10.1016/j.chemgeo.2004.04.026>.
- Woodhead, J., Stern, R.J., Pearce, J., Hergt, J., and Vervoort, J., 2012, Hf-Nd isotope variation in Mariana Trough basalts: The importance of “ambient mantle” in the interpretation of subduction zone magmas: *Geology*, v. 40, no. 6, p. 539–542, <https://doi.org/10.1130/G32963.1>.

SCIENCE EDITOR: AARON J. CAVOSIE  
ASSOCIATE EDITOR: JOCELYN MCPHIE

MANUSCRIPT RECEIVED 5 DECEMBER 2017  
REVISED MANUSCRIPT RECEIVED 26 JUNE 2018  
MANUSCRIPT ACCEPTED 31 JULY 2018

Printed in the USA